



REPORT: Final Report, Design of a whirling arm abrasive jet Micro-Machining apparatus operating in a vacuum

| | | | | | |
|--------------------------|-------------------|-------------------|----|--------------------|-------------|
| COURSE ID: | MEC 825 | SECTION #: | 01 | INSTRUCTOR: | Dr. V. Chan |
| COURSE TITLE: | Mechanical Design | | | | |

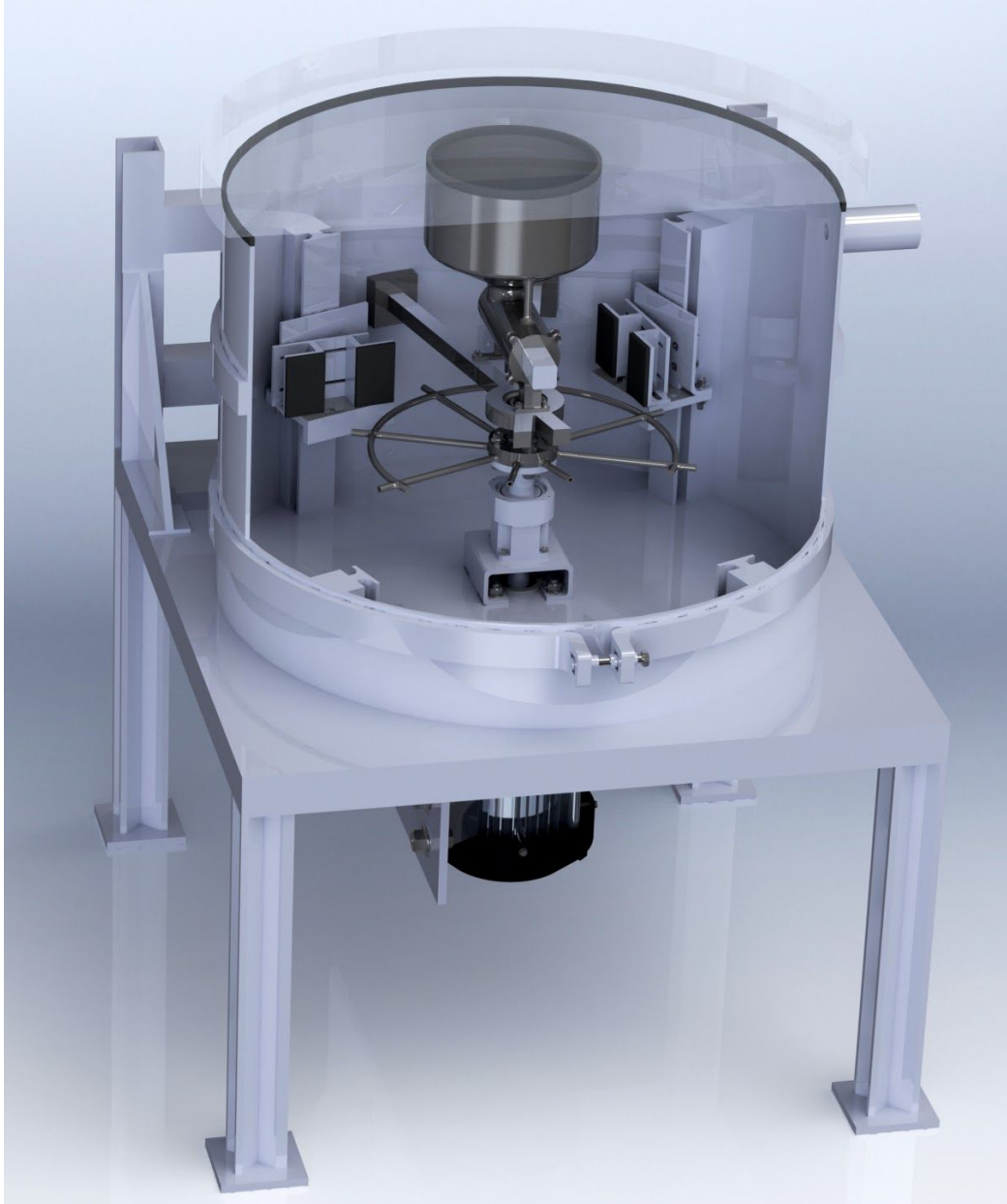
| | | | | | |
|--------------------|---------------|--|------------------------|---------------|--|
| GROUP ID: | Team CASE | | | | |
| SUPERVISOR: | Dr. M. Papini | | | | |
| DATE DUE: | 09-April-2019 | | DATE SUBMITTED: | 09-April-2019 | |

| NAME | STUDENT ID | SIGNATURE* |
|------------------------------|------------|---|
| Majid Eghbal | xxxxx3976 |  |
| Davin Cornelius | xxxxx0051 |  |
| Yalda Alemi | xxxx58274 | Y.A. |
| Sina Sartipzadeh Amirghasemi | xxxx01049 | S.S. |

(Note: Remove the first 4 digits from your student ID)

**By signing above you attest that you have contributed to this submission and confirm that all work you have contributed to this submission is your own work. Any suspicion of copying or plagiarism in this work will result in an investigation of Academic Misconduct and may result in a "0" on the work, an "F" in the course, or possibly more severe penalties, as well as a Disciplinary Notice on your academic record under the Student Code of Academic Conduct, which can be found online at: <http://www.ryerson.ca/senate/policies/pol60.pdf>.*

Winter 2020
MEC825: Mechanical System Design (Capstone)
FINAL DESIGN PROJECT REPORT



**Design of a whirling arm abrasive jet Micro-Machining apparatus operating
in a vacuum**

Team C.A.S.E

Abstract

Abrasive Jet micromachining is a process that can be used to machine hard and brittle materials like glasses and ceramics which are difficult to fabricate using conventional methods. Air jet is a focused stream of pressurized air that accelerates micro-abrasive particles to mechanically etch workpieces without producing heat and affecting workpiece's property. Usually, when the feature sizes are less than the jet footprint, a patterned masking technology is used to protect the substrate. However, for small mask openings, it is found that the jet stream results in channels that are shallower than wider ones; a phenomenon called 'Blast lag'. It is due to the fact that the brittle fracture of substrate is the predominant mode of erosion which results in forming V-shaped cross-sectional channels.

It is found that reducing the abrasive size will transform the erosion behaviour from ductile to brittle which further can eliminate the 'Blast lag' phenomenon and result in a U-shaped profile rather than V-shaped. Owing to that, the abrasive particle size must be reduced to below $10\text{ }\mu\text{m}$. However, at below $\sim <10\text{ }\mu\text{m}$, aerodynamic effects hinder the ability of the particles to strike the surface as the particles tend to follow fluid streamlines. The aerodynamic effects can be neglected if the machining process would be done in a vacuum.

In this Thesis, Team 'CASE' go through the design process to explore a mechanism/device that can overcome the problems mentioned above. The proposed design is a mechanism that utilizes a whirling arm, instead of an air jet, to accelerate the particles. The process will be done in a vacuum chamber to substantially reduce aerodynamic effects and it enables the device to run at a lower speed to accelerate the particles to desired speed. The design incorporates a feeding mechanism to feed the particles to the mechanism and includes 4 fixtures [jigs] to simultaneously machine 4 workpieces.

Figure 1: Schematics of the proposed Design

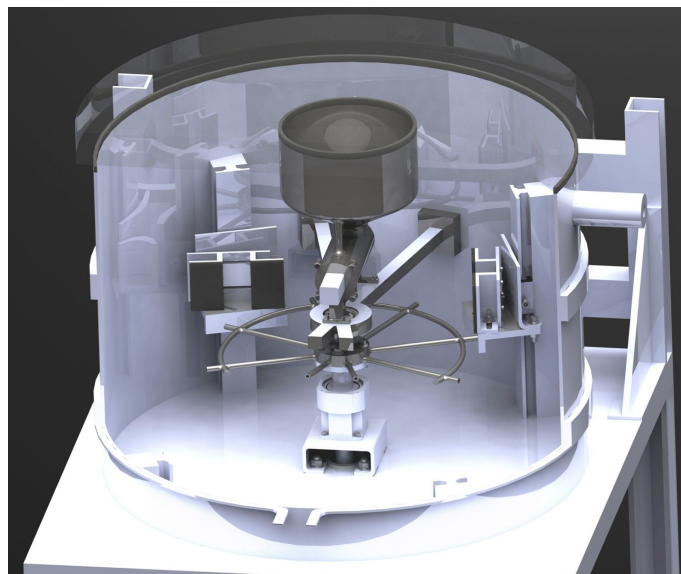


Table of Contents

| | |
|---|-----------|
| Abstract | 2 |
| Table of Contents | 3 |
| List of Figures | 6 |
| List of Tables | 7 |
| 1. Design Brief | 8 |
| 2. Problem Analysis | 9 |
| 2.1. Air Jet Machining Principles Regarding the problem | 9 |
| 2.2. Brittle-to-ductile erosion behavior transition for Abrasives | 12 |
| 2.3. Fluid motion in erosion by solid particle impact: | 13 |
| 3. Introduction | 15 |
| 4. Design Methodology | 16 |
| 5. Reference Design | 18 |
| 5.1. Our design Vs. Current solutions | 19 |
| 6. Literature Review | 20 |
| 6.1. Abrasive Material | 20 |
| 6.1.1. Selection of abrasive | 20 |
| 6.1.2. Abrasive Quality | 21 |
| 6.1.3. Recycling and Secondary Waste: | 23 |
| 6.1.4. Aluminum Oxide | 23 |
| 6.1.5. Shape | 26 |
| 6.1.6. Masking Technology: | 29 |
| 6.1.7. Material of the inner surface of the tubes: | 30 |
| 6.1.8. Material for masking the system | 31 |
| 6.2. Blaster | 33 |
| 6.3 Speed Requirement | 34 |
| 6.4. Feeder | 35 |
| 6.5. Enclosure | 38 |
| 6.5.1. Pressure Requirement & Modeling of Particle speed in air | 38 |
| 6.5.2. Device Selection | 39 |

| | |
|---|-----------|
| 6. Requirements | 41 |
| 7. Systems | 43 |
| 7.1 Major Component Listing | 44 |
| 7.1.1 Blaster System | 44 |
| 7.1.2 Containment System | 44 |
| 7.1.3 Power System | 45 |
| 8. Detailed Design | 47 |
| 8.1. Sample calculations: | 47 |
| Prediction of required abrasive mass flow rate: | 47 |
| Calculating speed and angle of particles shooting out of the blaster wheel: | 52 |
| Calculating required torque to maintain the wheel speed | 56 |
| Calculating Start-up torque | 58 |
| Calculating the maximum moment applied on the shaft due to eccentricity | 59 |
| Calculating the diameter of the shaft | 60 |
| Vibration Analysis of the system | 67 |
| Heat transfer analysis on Gearbox | 74 |
| Pressure Requirement & Modeling of Particle speed in air | 77 |
| 9. Conclusion and Recommendation | 79 |
| References: | 80 |
| 10. References | 81 |
| Appendix A | 85 |
| A1 code for calculating the drag experienced by the particles (MATLAB) | 85 |
| A2 code to calculate speed of impact of particles (Python) | 86 |
| Appendix B: CAD Drawings | 89 |

List of Figures

| Figure # | Title | Page # |
|-----------------|---|---------------|
| 1 | Schematics of the proposed Design | 2 |
| 2 | The indentation process giving micro cracks | 9 |
| 3 | A photograph of the imprints of the crack patterns | 10 |
| 4 | Typical curves showing the variation of erosion with impact angle | 10 |
| 5 | Gas streamlines and particle trajectories particles for the case in point | 12 |
| 6 | Impinging jet and and particle trajectory | 13 |
| 7 | The Design process Spiral | 17 |
| 8 | Reference designs | 19 |
| 9 | Blocky shape (High Bulk density) | 26 |
| 10 | Blocky shape (Medium Bulk density) | 27 |
| 11 | Sharp shape (Low Bulk density) | 27 |
| 12 | Mass loss rate of Hardide compared to leading hard surfacing material while being tested by aluminum oxide as the abrasive material | 30 |
| 13 | hardness, toughness and wear resistance of tungsten carbide | 31 |
| 14 | Wheel blasting diagram | 32 |
| 15 | Lobe Pump Diagram | 35 |
| 16 | Centercore Auger | 36 |
| 17 | Flat wire, beveled wire, square bar, and round wire screw profiles | 36 |
| 18 | Diagram of all systems and designed components | 42 |
| 19 | Shows the MSMD082S1U motor used in the design | 44 |
| 20 | The torque speed curve of the MSMD082S1U motor | 45 |
| 21 | Shows the ATEX GXA series gearbox. | 45 |

| | | |
|----|--|----|
| 22 | Shows the NS-DF-2 Sealed bearing. This bearing can be adjusted between 25 and 51 mm | 46 |
| 23 | The erosion efficiency of glass plotted against the kinetic energy of the individual particle for a wide range of erodent sizes, velocities and a range of erodent materials | 47 |
| 24 | a)schematic of the channels and b) cross-sectional area of the erodant channel | 48 |
| 25 | Top view of the chamber, showing the position of the samples with regard to the centre of the chamber. | 49 |
| 26 | Mass flowrate versus channel width (Aspect ratio of 1:1) | 50 |
| 27 | schematic of the particle and its corresponding velocity as it travels in the tube | 51 |
| 28 | Top view of the schematic showing position of the particle | 51 |
| 29 | the Matlab code used to iteratively calculate radial velocity of the particle | 52 |
| 30 | schematic of the particle and the corresponding forces acting on it | 55 |
| 31 | Schematic showing placement of the wheel and shafts | 60 |
| 32 | Schematic of the single degree of freedom system, vibration induced by rotational mass unbalance | 67 |
| 33 | simulation of the systems' vibration without any external dampers | 69 |
| 34 | z-axis is the vibration amplitude for different values of μ and β | 70 |
| 35 | this figure shows the vibration of the system for $\mu=45$, $\beta=23$ | 70 |
| 36 | combinations of μ and β that do not pass the criteria | 71 |
| 37 | The schematic of gearbox assembly and its corresponding conduction resistance network | 74 |

List of Tables

| Table # | Title | Page # |
|----------------|---|---------------|
| 1 | Compared the shortcomings of each of the preexisting designs, and how ours improves upon them. | 20 |
| 2 | Abrasive Media for Microabrasive Cleaning and Processing Applications | 21 |
| 3 | Surface roughness of NiTi specimen as a function of abrasive size and blasting pressure | 25 |
| 4 | typical physical properties of white Aluminum Oxide | 28 |
| 5 | Results of erosion by alumina hard particles carried by gas jet at 70 m/s | 30 |
| 6 | Shows the values for finding the kinetic energy of AF 45 glass. | 33 |
| 7 | Minimum impact velocity to cause lateral cracks | 33 |
| 8 | Material Properties used for generating table 7 | 34 |
| 9 | Assumes an initial launch at 275 m/s, the resulting speed is tabulated below | 38 |
| 10 | Blaster Component listing | 44 |
| 11 | Containment system Component listing | 45 |
| 12 | Power System Component listing. | 46 |
| 13 | Mass flow rate needed in (gr/min) for variety of channel width, assuming the process must be over in less than 10 minutes | 49 |
| 14 | Radial speed, Total speed, and departure angle based on different coefficient of friction at 9500 RPM. | 53 |
| 15 | Moment of inertia of rotating components | 57 |
| 16 | The outer diameter of the hollow shaft(mm) based on the eccentricity and material | 66 |
| 17 | Assumed values for Systems Vibration analysis | 68 |
| 18 | Thermal resistance of components | 75 |

1. Design Brief

Abrasive jet micromachining uses a jet of compressed fluid to accelerate micro-abrasive particles to high speeds. The jet impinges a target which has been covered with an erosion resistant masked pattern in order to create features such as microchannels, etc. It has been found that more accurate and smaller features can be made if the size of the abrasive particles is decreased. However, at below $\sim < 10 \text{ um}$, aerodynamic effects hinder the ability of the particles to strike the surface as the particles tend to follow fluid streamlines. This difficulty could be overcome if the machining was performed in a vacuum. To this end, the team will design a whirling arm apparatus to launch the particles, and a vacuum chamber in which to perform the machining. Possible avenues for feeding the particles into the whirling arm will also be explored.

2. Problem Analysis

2.1. Air Jet Machining Principles Regarding the problem

The knowledge on solid particle erosion has been used for the development of a new micro-machining technology, abrasive jet micro-machining or called micro abrasive jet machining (MAJM). This is a high efficient and low cost machining technology for brittle materials such as glasses, silicon and ceramics with broad applications in semiconductors, electronic devices, MEMS, flat display panels, and microfluidics [1]. In particular, MAJM has been an effective means for the fabrication of micro-channels and holes on brittle glasses. In MAJM, fine particles are accelerated in an air or gas stream and directed towards the target material. When a particle impacts the surface of a brittle material, it causes an impact fracture to the material and a material removal mostly by crack propagation.

The basic event in the mechanical etching process is a single abrasive particle hitting the substrate material. Usually hard, angular particles are utilised in the process. When such a particle hits the substrate material, high compressive stresses arise around the impact site, giving rise to a plastically deformed zone see Fig. 1 . At high impact velocities, the tensile stresses around the plastic zone start initiating micro cracks. Two families of cracks are generated, so-called lateral cracks parallel to the substrate surface and radial median cracks into the substrate. The lateral cracks give rise to chipping of substrate material resulting in the actual etching. The radial cracks run into the substrate causing a decreased strength of the substrate. Fig. 2 shows an example of the imprints, the two cracks patterns leave after erosion. [2]

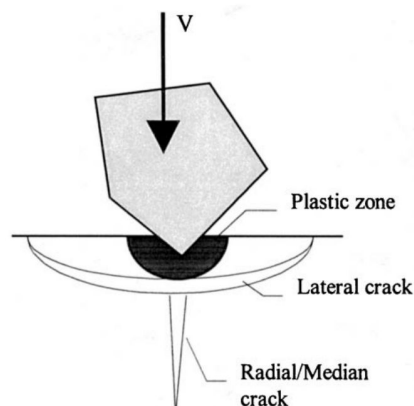


Figure 2: The indentation process giving micro cracks [Slikkerveer 2000][2]

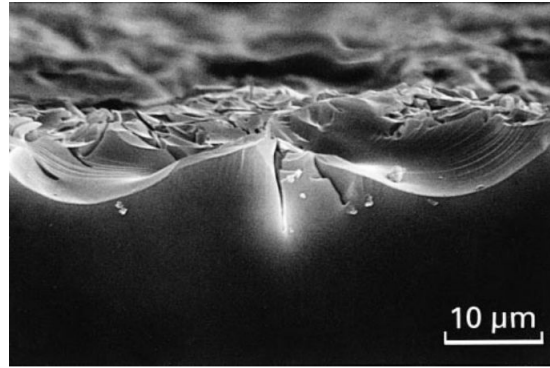


Fig 3: A photograph of the imprints of the crack patterns. [Slikkerveer 2000][2]

Based on the conducted studies on both ceramics (brittle materials) and metals (ductile materials), it is suggested that the impact angle was the most significant indicator of the erosion mechanism [3]. Ductile materials show the greatest wear rate at a shallow impact angle, while brittle materials wear most rapidly when the particles are incident normally to the Surface. It was found that the two parameters that most influenced solid particle erosion in the case of metals, ceramics and polymers were the impact angle and the hardness of the target. [4]

Erosion rate of a target material at a certain impact angle depends on the ductility of the material if other experimental variables are kept constant. It is clear that the more ductile the material, the higher is the maximum normalized erosion and the shallower the impact angle at which the maximum occurs. As shown in Figure 3, the ceramic material showed a brittle characteristic having a maximum erosion rate at normal impact.

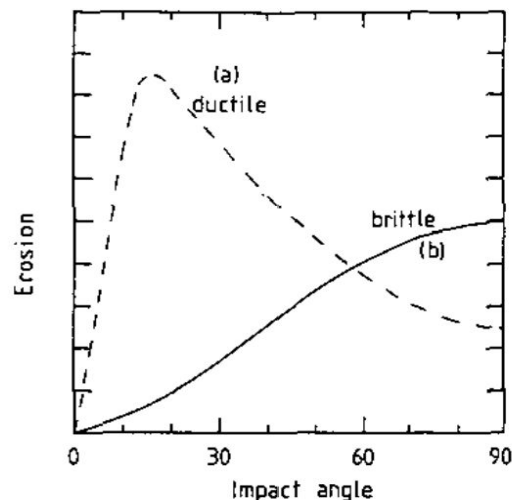


Figure 4: Typical curves showing the variation of erosion with impact angle: (a) for ductile metal; (b) for a brittle material eroding by fracture.

In Abrasive jet micromachining of brittle substrates, if the feature sizes are less than the size of the abrasive jet footprint, then a patterned erosion-resistant mask is used to protect the substrate material, leaving exposed areas to define the features. Previous investigations have revealed a ‘blast lag’ phenomenon in which, for the same dose of abrasive particles, narrower mask openings lead to channels that are shallower than wider ones. Blast lag occurs when using AJM on brittle substrates because of the natural tendency to rapidly form a V-shaped cross-sectional profile which inhibits abrasive particle strikes on the narrow vertex at the feature centerline.[7]

Blast lag occurs only in brittle erosive systems, where the V-shaped channel rapidly results because the erosion rate is higher at normal incidence (flat channel center) compared to on the sloped sidewalls [5]. For ductile erosive systems, the much higher erosion rate at oblique incidence (channel sidewalls), compared to normal incidence (channel center) results in a U-shaped cross-section [6] which is not subject to the blast lag phenomenon. “Wensink and Elwenspoek (2002) [5]” noted that blasting with the jet oblique to the target can reduce the blast lag in straight channels or holes since the material removal rate on the flat feature bottom is decreased relative to the sidewalls, thus extending the “stage I” erosion when the feature remains bowl shaped [5]. The net result of blasting across a feature at oblique incidence is that a more U-shaped feature results, which is slightly less prone to blast lag.

To overcome the “Blast Lag” phenomenon, it can be suggested that if the abrasive particles show more of a ductile behaviour, U-shaped channels can be created rather than V-shaped cross sectional profile. Sheldon and Finnie (1966) [9], for example, found that commercial pure aluminium followed curve Fig 3-(a), while soda-lime glass, sintered magnesia, sintered alumina, moulded graphite and hardened tool steel all showed behaviour similar to curve (b). Similar dependence of erosion rate on impact angle for ceramics and other nominally brittle materials has been observed in many subsequent studies. Behaviour following curve (b) in figure 3 is therefore commonly referred to as ‘brittle’ erosion behaviour.

2.2. Brittle-to-ductile erosion behavior transition for Abrasives

Sheldon and Finnie (1966) [9] also, however, demonstrated clearly that ‘brittle’ angular dependence (curve (b)) is not inevitably seen in ceramics and other ‘brittle’ materials. They showed that on reducing the size of the silicon carbide erodent particles from $\sim 125 \mu\text{m}$ to $\sim 9 \mu\text{m}$, the angle of maximum erosion for soda-lime glass, moulded graphite and magnesia shifted from close to 90° to a much lower angle: the behaviour had changed from ‘brittle’ to ‘ductile’. This phenomenon corresponds to a genuine transition from brittle (i.e. brittle fracture-dominated) to ductile (i.e. plasticity dominated) behaviour, as the size of the erodent particles is reduced.

In conclusion, It has been found that more accurate and smaller features can be made if the size of the abrasive particles is decreased. However, at below $\sim 10 \mu\text{m}$, aerodynamic effects hinder the ability of the particles to strike the surface as the particles tend to follow fluid streamlines. However, new methods for accelerating and launching the abrasive can be explored to achieve the desired features.

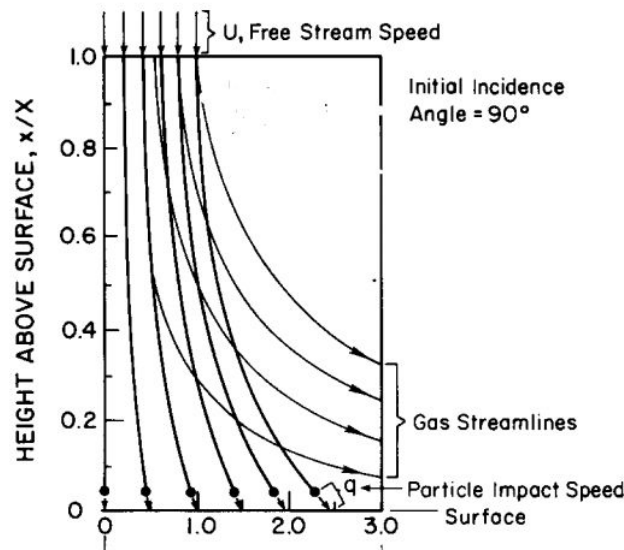


Figure 5: Gas streamlines and particle trajectories particles for the case in point
[Humphrey 1990] [10]

2.3. Fluid motion in erosion by solid particle impact:

Surface erosion of material by solid-particle impact is a problem in nature and many multiphase flow industrial devices. Here, we are concerned with the latter, especially in the context of airborne abrasives. Figure 7 shows the flow configurations frequently encountered in solid particle erosion practices. The impinging jet geometry shown in Figure 7 spans a variety of applications, ranging from research into resistance of materials to wear to metal cutting.. The anticipated dynamic behavior of large and small particles of the same material is loosely interpreted in Figure 7. The ability of a particle to respond to changes in fluid velocity and so alter its trajectory is characterized by its momentum equilibration number, λ . It is defined algebraically by Equation Em 1 and is the ratio of two time scales that characterize the dynamics of the solid and fluid phases, respectively. Here, we simply note that particles with $\lambda \gg 1$ are highly inertial and very slow to respond to changes in fluid velocity. In contrast, particles with $\lambda \ll 1$ faithfully follows the flow and, in principle, could be used to visualize fluid motion. [10]

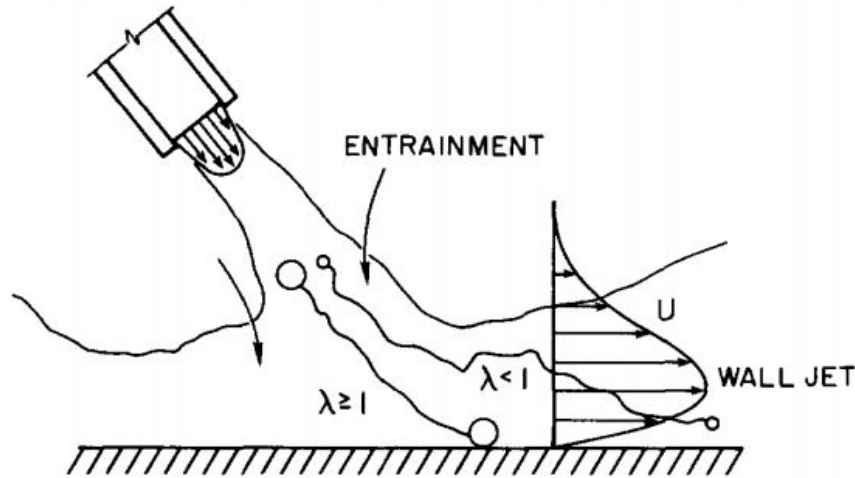


Figure 6: Impinging jet and particle trajectory [Humphrey 1990] [10]

$$\lambda = \frac{\tau_p f_D}{\tau_f} \quad \text{Eq: Em1}$$

Or for $f_D = 1$ $\text{Stokes number} = \frac{\tau_p}{\tau_f} \quad \text{Eq: Em2}$

For low Reynolds, corresponding to creeping flow, λ becomes identical to the "inertia" or Stokes number. A particle with a low Stokes number follows fluid streamlines (perfect advection), while a particle with a large Stokes number is dominated by its inertia and continues along its initial trajectory. For acceptable tracing accuracy, the particle response time should be faster than the smallest time scale of the flow [32].

This issue becomes predominant when using air jet stream to shoot substantially small particles, ~ 5 . Their corresponding stokes number will be $\lambda \ll 1$ which means that the particles travelling towards the surface will be affected by the stagnation pressure next to the surface and follow the jet streamline rather than hitting the subject.

3. Introduction

To design an abrasive machining system there are many considerations that need to be made. The most key is the material that we are to machine, as that will dictate what methods we should research. Second is the complexity of shapes to be machined. Of the two we have defined AF-45 borosilicate glass as the material, as it is consistent with the professor's current research and has use in industrial settings. The complexity of the shapes are to be hole with a square shape base (not a v shaped crack), and if possible square shaped channels. We have gone in depth explaining why this is a challenge with current machinery. To make such shapes possible it is needed to use small particle sizes which will be prone to aerodynamic effects such as drag considerably. For this reason a vacuum setup is needed and numerical analysis has been performed to define the pressure needed by reducing drag force on particles. To become knowledgeable about how the machine will feed in the abrasive research was done on aluminum oxide as an abrasive, while also looking into various delivery methods that keep the abrasive from clumping together. Finally research was done on what speed the particles need to achieve and what mechanism can allow us to reach this.

3.1 Device use description

Here we have summarized how the device is meant to be used and what the user will encounter when operating the machine. We will go through initial setup, placing in samples and running the device.

The user will first place the vacuum chamber onto the provided table and lock the two together using the belts. The belts are tightened with screws on the perimeter of the belt. The unit itself is not expected to vibrate much but the care should be taken to tighten the belts firmly. Not allowing the chamber to slide out. Next the motor should be connected to the bottom of the chamber and its shaft locked onto the adjustable bearing. The bearing provides an airtight fit around the shaft.

Assuming the components inside the chamber have been assembled a priori, the user can now take out the sample holder from the fixtures on the perimeter of the chamber walls. The sample can be placed onto the jig holder and using screws held on. The holder has been designed to allow for a variety of shapes and user can place the sample however they want. The only key part is to the sample and the desired angle relative to the backing at this point and have the sample tightened onto the holder. The user can now slide the holder back in and by placing the brakes around the holder and tightening the screws around it hold the unit in place.

At this point the samples are ready to be blasted, it is best to leave pouring in the abrasive to the last second as humidity can cause the sand to clump up. The user can now pour the abrasive into the upper chamber. Before pouring the abrasive all final checks should have been done and now the acrylic lid should be tightened onto the unit, making sure the sealing ring is in place.

The user can now start the motor for the abrasive feeder mechanism allowing for the abrasive to be agitated. At this time the vacuum pump can also be started. At full vacuum the main motor can be spooled up to allow for cutting to begin. The unit has been designed for a 2000 RPM motor speed to be enough for cutting borosilicate glass.

4. Design Methodology

[This section is courtesy of Dr. Filippo A. Salustri' Design site [11]]

The Design methodology used for this project is the “Design Spiral” approach which is mainly a systematic procedure to address the imbalances in the as-is situation. The design “spiral” is shown in figure 4. It's based on three major stages – problem analysis, system design, and concept design – which are repeated recursively at successively finer/lower levels of detail [12]. At each successively lower level of detail, these three stages repeat – the steps remain the same – but on “different” problems at each level.

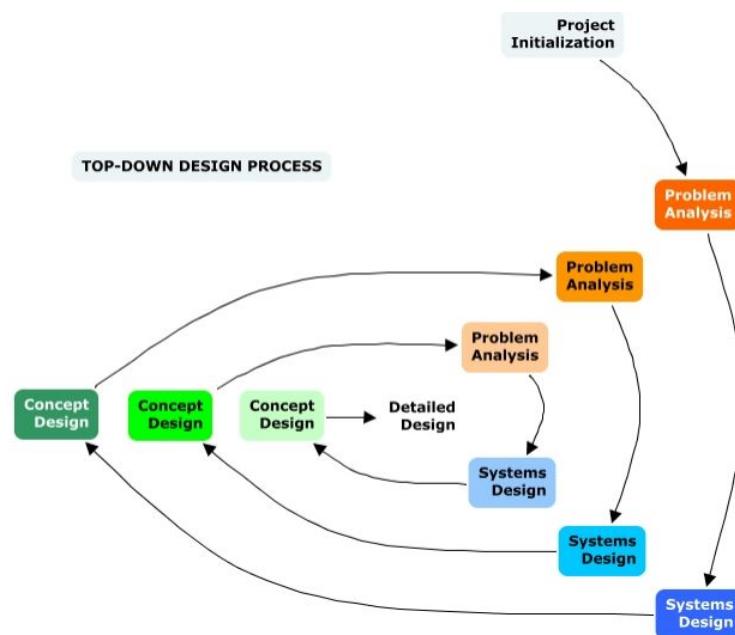


Figure 7: The Design process Spiral [Courtesy of “Fil Salustri's Design Site” [12]]

In the First stage, Problem Analysis, our team will explore and understand the context in which the intervention will have to operate and find the imbalances. Following that, the inputs/outputs to the system and a list of context transformations will be identified. Later, these transformations will capture a form of preliminary requirements that our intervention will meet.

Moreover, in the second stage, System Design, a list of systems that can address the requirements will be identified. At this stage, the intervention will still be assumed as a black box with a set of transformative functions. Furthermore, an analysis will be conducted to follow the flow if input through those systems to become the expected output.

The last stage, Concept Design, is basically Embodying all those systems as a physical principle or technologies that can perform the required transformation functions. Eventually, all the embodiments will be presented as an implementable design including CAD design and Drawings.

5. Reference Design

An example of several similar enclosures used for such a situation is placed in Figure 2. The reader should note that such an enclosure however does not need to meet the vacuum sealing capabilities of our design. Even though all but the Wazer devices are air tight, none have been prepared for a quick vacuum creation. Meaning the enclosures are too big for the purposes they are intended for and take up time for creating a vacuum.



A.



B.



C.

Figure 8: Reference designs: .(A) Shows the Water jet machining system by WAZER[1] (B) Comco automatic blasting machine[2]. (C) Gritco Vacuum Blasting machine[3].

5.1. Our design Vs. Current solutions

Table 1. Compared the shortcomings of each of the preexisting designs, and how ours improves upon them.

| Shortcomings of Advanced Lathe | Shortcomings of Gritco | Shortcomings of Wazer | OUR DESIGN |
|---------------------------------|--|------------------------|---|
| Limited viewing of the specimen | Lack of machining capabilities | Limited user interface | Full viewing capability |
| Unused space | Cannot accurately pinpoint area of contact | | Vacuum sealed environment |
| Lack of vacuum seal capability | | | User interface on device |
| | | | Large enough to allow for the required piece size |
| | | | Portable design |

As seen in Table 1, our design tries to meet the need for vacuum by making the enclosure as small as can be, and fit the needed equipment for machining. It is key that the design be portable in a lab, as that would allow the user to connect it up to their own custom equipment. A major problem of most designs is that the user interface was not available on the unit, this should be fixed, for modern equipment since most 3D motion devices allow for quick connection of a USB with G code to run a project.

6. Literature Review

6.1. Abrasive Material

6.1.1. Selection of abrasive

The selection of the abrasive depends on the type of the action that the material is going to execute on the working surface. The impact of the abrasive material depends on three key characteristics [13]:

- Particle shape: The shape of the abrasive can be angular, spherical, blocky or semi-round. Angular, sharp particles cut and strip the surface and are proper for making deep profiles. On the other hand, round and spherical particles are slower and are proper for pounding and peening a surface and making shallower profiles.
- Hardness: This measurement is done using the Mohs scale. Harder particles will remove the material more aggressively and faster.
- Particle size: Larger particles remove the material faster and because they generate a greater kinetic energy for the same speed, they produce a heavier texture or a rougher surface.

Table 2: Abrasive Media for Microabrasive Cleaning and Processing Applications [13].

| Abrasive | Hardness (Mohs scale) | Average Particle Size (μm) | Description/Characteristics | Applications |
|--|-----------------------|---|---|--|
| Diamond | 10 | 0.25-5 | Diamond has the highest hardness known. The small particle size makes it possible to achieve high-quality surface finish and high-precision micromachining | Processing of hard metals and ceramics |
| Cubic boron nitride (CBN) | 9.5 | 1-10 | CBN has the second highest hardness known. The small particle size makes it possible to achieve high-quality surface finish and high-precision micromachining | Processing of hard metals and ceramics |
| Silicon carbide (SiC) | 9.3 | 20-60 | This is the most aggressive powder used for microabrasive blasting. It is typically used when very fast material removal is a requirement | Cutting, deburring, drilling, texturing, fossil preparation, wafer fabrication |
| Aluminum oxide (Al_2O_3) | 9 | 12-165 | Alumina is the most commonly used cutting abrasive. The shape and hardness of the particles make it an excellent choice when working with metals or hard, brittle parts | Intricate cutting; hole and slot drilling; surface preparation; fine surface finishes; heavy deburring; large-scale rust removal; wafer fabrication; surface texturing; fossil preparation |
| Crushed glass | 5.5 | 50-60 | Crushed glass results in a material that works well as a mild abrasive. It has the hardness of glass bead with numerous shard-like edges. Crushed glass is most often used when only a light degree of abrasion is required | Light cleaning; surface finishing; epoxy removal; mineral preparation; restoration of artifacts |

6.1.2. Abrasive Quality

The powder blasting process strongly depends on the quality of the abrasive. The three main factors that impact the quality are as follows [13]:

- a. Moisture: The average size of the particle of a micro abrasive particle ranges from 0.25 to 200 μm . As the size of the particle decreases, the ratio of the surface area to volume increases. Therefore, moisture is absorbed by the particles and would cause them to clump and stick together. These clumps will cause uneven flow and even total blockage. This is an important factor and should be concerned specially for designing the feeder [13]. Industries have special methods for preventing clumps in their packages for storing and transporting the abrasive materials. For example they pack the material in heat-sealed bags and containers for protection against contamination and moisture [15].
- b. Foreign Particles: Due to the small size of the orifices and nozzles in the design, the sensitivity of the design to contaminants and any impurity increases. Contaminants such as fiber, plastic and even wood must be removed to produce a pure and effective blasting powder [13].
- c. Particle Size Distribution: A high-quality powder has a narrow range of particle size and would only have few outliers. The extremes strongly affect the quality of the powder. The coarser particles might block the way and if not, will affect the surface more aggressively. Very fine particles can be equally damaging. As mentioned earlier, finer particles tend to be more sensitive to moisture. They will also fill in the space between larger particles and as the air is removed, the particles will pack together more tightly and the energy required to make the medium flow effectively will increase. Even worse, the clump can stop the flow and cause blockage [13]. Standard sizes of these materials and approved testing methods are defined in ANSI B74.20-2004, currently under pre-publication formatting as of this writing. In general, standard sizes for these materials are defined as a size range (e.g. 1-2 microns, 6-12 microns). The standard specifies that

materials in these sizes must include at least 90% of the particle size distribution within the size ranges specified (maximum of 5% each above and below the range). For example, for a 1-2 micron size, at least 95% of the sample must be above 1 micron in size, and no more than 5% of the sample may be over 2 microns in size. The sample's average size must be near the center of the desired distribution (1.28-1.72 microns for a 1-2 micron material). Additionally, the coarsest particle detected must be below a maximum limit (e.g. 6 microns for size 1-2, 20 microns for size 6-12) [14].

To maintain high quality, the size distribution must be standard and accurate. Also, the environment must be humidity- and temperature-controlled especially in the feeder. The design of the feeder must be utilized to prevent clumps and provide a smooth flow [13].

6.1.3. Recycling and Secondary Waste:

Micro Abrasive jet machining has this limitation of only using the abrasive for only one cycle. Used material can not be reclaimed and reused due to the following reasons [16]:

- a. The abrasive breaks down easily after the process. Hence, the size range and variety of the particles will be greater. The cutting force of the particles will change respectively and process reliability can not be assured.
- b. When the abrasive is exposed to air it will readily absorb moisture and negatively impact the process as mentioned. Although, in a vacuum chamber this factor will not be a major concern.
- c. Fragments of the substrate get mixed in with the abrasive, resulting in contamination and impurities in the powder which changes abrasive characteristics of the medium.

The use of dry abrasive powders eliminates the need for aqueous cleaning agents, which are difficult and expensive to process and dispose of. None of the available abrasives generates additional secondary waste. Sodium Bicarbonate and dolomite are also water soluble, making waste treatment and handling easier. The expensive abrasives, such as diamond and boron nitride, can be recovered from the waste stream with optional patented separation systems for use

in other applications. Depending on the abrasive and the waste stream, different aqueous or non-aqueous waste separation methods, such as electro-static precipitation, electroacoustic separation or flocculation, are used to separate and recover the abrasives [16].

6.1.4. Aluminum Oxide

Alumina is the main abrasive used for grinding, lapping and polishing. Considering the applications that have been mentioned previously, aluminum oxide is the best candidate for the purpose of this project and suits the requirements perfectly. Its abrasive characteristics are formed during the furnacing and crushing operations. There are four types of gradation for toughness. The toughness does not increase the duration of wearing. If the grain is too tough for a process it will become dull and will rub the work. Increasing the friction, creating heat and vibration. On the other hand, a grain that is too friable will wear away rapidly, shortening the life of the abrasive tool. There is a range of grain toughness suitable for each application. The slower the cooling process, the larger the crystals are which are more friable compared to the finer ones. Hence, to obtain very fine crystals, the charge is cooled extremely rapidly. Alumina abrasives are derived either by electrofusion, or by chemical precipitation and/or sintering [17].

White aluminum oxide is one of the most popular grades for micron-size abrasive because of its versatility for a wide range of material. To produce micron sizes, alumina is ball-milled or vibro-milled after crushing and then traditionally separated into different sizes using an elutriation process. This consists of passing abrasive slurry and water through a series of vertical columns. The width of the columns is adjusted to produce a progressively slower vertical flow velocity from column to column. Heavier abrasive settles out in the faster flowing columns while lighter particles are carried over to the next. The process is effective down to about 5 μm and is also used for micron sizing of SiC. Air classification has also been employed. White 99% pure aluminum oxide, called mono corundum, is obtained by sulphidation of bauxite, which outputs

different sizes of isometric corundum grains without the need for crushing. The crystals are hard, sharp, and have better cleavage than other forms of aluminum oxides, which qualifies it for grinding hardened steels and other tough and ductile materials. Finer-grain aluminum oxide with a good self-sharpening effect is used for finishing hardened and high-speed steels, and for internal grinding [17].

As indicated, each particle size is appropriate for a particular job and impacts the surface roughness at the end. The following table illustrates the results of blasting with 3 different particle sizes of 17.5 μm , 25 μm , and 50 μm for three different blasting pressures. The specimen was micro blasted for 30 seconds and Aluminum Oxide was used for this experiment. It can be seen that changing the size of the particle has a greater impact on the surface than the blasting pressure [18].

Table 3: Surface roughness of NiTi specimen as a function of abrasive size and blasting pressure [18].

| Al ₂ O ₃ Pressure (psi) | Average Surface Roughness (nm) | | |
|--|--------------------------------|--------|--------|
| | 17.5 | 25 | 50 |
| 80 | 244 | 397.32 | 606.78 |
| 100 | 281.66 | 410.3 | 756.96 |
| 120 | 325.55 | 392.46 | 611.53 |

6.1.5. Shape

The shape of the particle is one of the important factors affecting the performance of the abrasive in several ways, such as rate of material removal and level of subsurface damage. For many of the abrasives, the aspect ratio (length to width) is a primary descriptor of shape. Fused aluminum oxide tends to have one long dimension and two smaller, roughly equal dimensions; i.e., the thickness is roughly equal to the width. Calcined alumina tends to have two long dimensions and one much smaller one; i.e. the length and width are roughly equal, but the thickness is about one-fifth the length. (For calcined alumina, this ratio, length to thickness, is often referred to as the aspect ratio). For more exotic shapes, aspect ratio may vary with the size of the particle and thus can only be given as a range. The following figures illustrate different shapes of the particle [14].

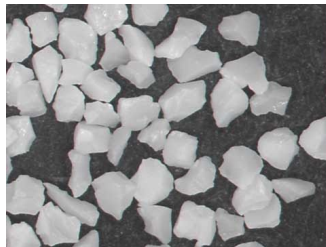


Figure 9: Blocky shape (High Bulk density) [14].

a. Blocky Shape (High Bulk density) - The abrasive grain is "rounded" by abrading equipment to remove very sharp, weak grain. Depending on application, the grain shape can vary from "mulled" to blocky with sharp edges. The blocky shape enhances the toughness and bulk density of the grain. Applications include tougher grinding or sanding applications, longer life for sandblasting and increased density for refractory or ceramic applications. Aspect ratio is approximately 1:1 [14].

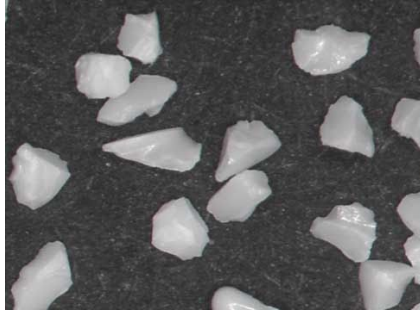


Figure 10: Blocky shape (Medium Bulk density) [14].

b. Blocky Shape (Medium Bulk density) - The abrasive grain is shaped to yield particles which are sharp but do not contain weak, platey or needle-like particles. Uses include general grinding, sanding, sandblasting and refractory applications. Aspect ratio is approximately up to 1.5:1 [14].

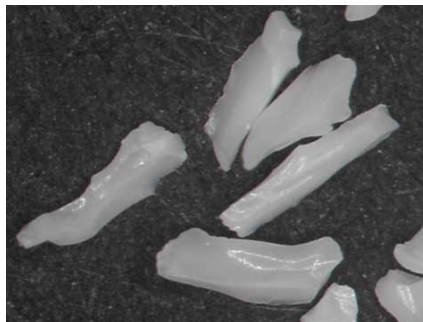


Figure 11: Sharp shape (Low Bulk density) [14].

c. Sharp Shape (Low Bulk density) - Abrasive grain that has been specially crushed to yield very sharp grain. This is generally required by the Coated abrasives industry and some grinding wheel applications to produce an aggressive, fast cutting product. Aspect ratio ranges from 1.5:1->3:1 [14].

White Aluminum Oxide Properties

The following table contains typical physical properties of white Aluminum Oxide that is important for the blasting process.

Table 4: typical physical properties of white Aluminum Oxide [19].

| | |
|-------------------------------|---|
| Crystallography | Alpha alumina, in a hexagonal crystal |
| Color | White |
| Specific Gravity | 3.96 |
| Knoop ₁₀₀ Hardness | 2000 |
| Shape | Blocky, with sharp edges |
| Grading (Grain) | ANSI B74.12-2001, Table 2 OR FEPA 42-1:2006 |
| Grading (Powder) | ANSI B74.10-2001 OR FEPA 42-2:2006 |
| Bulk Density (Grain) | ANSI B74.4-1992 (R2007) |

6.1.6. Masking Technology:

Metal Masks:

Parts of the enclosure need to be masked in order to be protected from erosion. Ductile materials like metals, have a low erosion rate which makes them suitable for masking purposes. They can also be magnetically clamped or by using an intermediate protection/adhesion layer. A metal layer with sufficient thickness will last long and is an appropriate option for masking. The disadvantage of this type of masking is the limitation that it puts on the features. In the case of using it permanently to protect the enclosure, this will not be an issue. Electroplating can be used as an intermediate adhesion to stick the metal on the targeted surface [20].

Elastomer Masks:

The erosion mechanism of rubber-like materials significantly depends on whether it is brittle or ductile. No lateral cracks appear on elastomer masks unlike brittle materials. The erosion mechanism of elastomer masks is based on fatigue and therefore, they provide high erosion resistance. Although, the behavior of the elastomers is a function of temperature, rate of deformation and particle velocity [20].

Overall, in order to achieve a perfect erosion resistance coating for various velocities and impingement angles, a combination of extreme hardness and enhanced toughness is needed. Hard and brittle materials have a very low erosion resistance when they are subjected to angles close to 90 degrees. On the other hand, ductile but tough metals lack hardness and are eroded more easily at lower impingement angles of 30 degrees because of ploughing and cutting effects. During the process, the particles are going to attack the surface from different angles and it is hard to prevent this action. Although by right combination of hardness, toughness and compressive stresses, the mask will be erosion resistant for different impingement angles [21].

There are several companies producing materials with low erosion rates to be used for masking. For instance, Hardide Coatings, is one of the leading providers of advanced tungsten carbide coatings that noticeably increase the life of metal parts operating in abrasive, erosive and corrosive environments. Erosion resistance tests were performed in accordance with ASTM G76-95, a test method used to rank the erosion resistance by solid particle impingement. Abrasive particle velocity was 70m/sec and aluminium oxide (particle size 50 microns) was used. The following graph illustrates the results of testing the Hardide and other materials at various impingement angles. The Hardide coating erosion rate was 0.017 – 0.019 mm³/g which is significantly better than the erosion rate of the tested types of cemented carbide, white iron, hard chrome and chrome carbide weld overlay. It can also be seen that in this experiment the Hardide coating resists erosion three times better than steel and more than twice than cemented carbide, hardmetal [21] .

Figure 12: Mass loss rate of Hardide compared to leading hard surfacing material while being tested by aluminum oxide as the abrasive material [21].

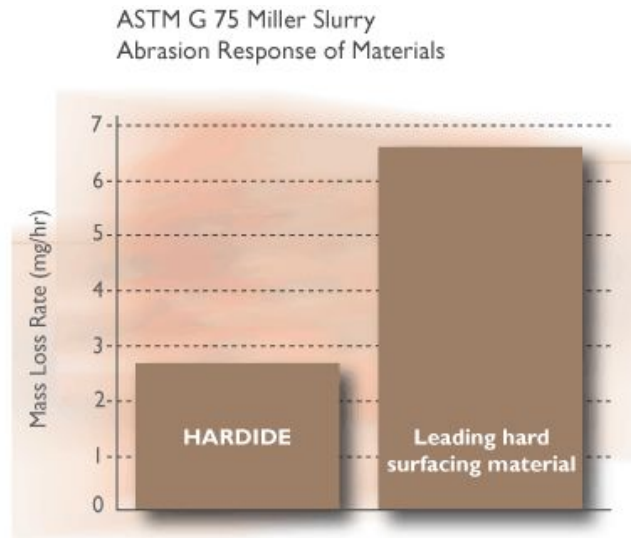


Table 5: Results of erosion by alumina hard particles carried by gas jet at 70 m/s [21].

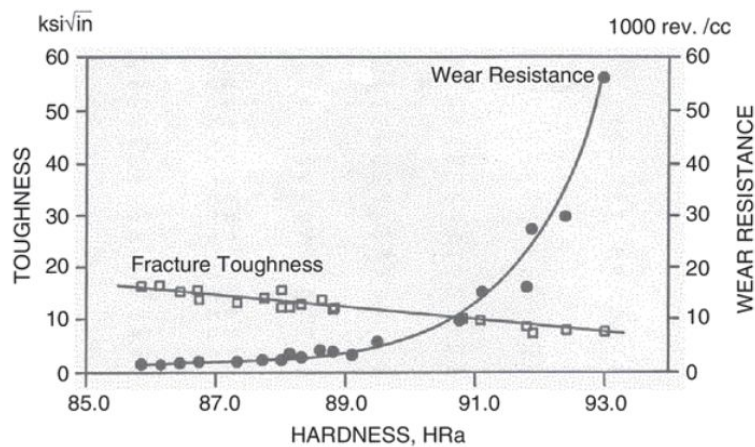
| Angle of target ° | Erosion Rate, mm ³ /g*1000 | | | | | |
|----------------------|---------------------------------------|-----------------------------|------------|---------------------------------|-------------|-------------|
| | Hardide | Chrome Carbide Weld Overlay | White Iron | AR-500 Abrasion-resistant steel | WC cladding | Hard Chrome |
| 45 | 19 | 71 | 76 | 53 | 36 | 25 |
| 60 | 18 | 66 | 64 | 48 | 41 | 26 |
| 90 | 18 | 60 | 40 | 40 | 50 | 30 |

6.1.7. Material of the inner surface of the tubes:

As the abrasive particles travel through the tubes, the inner surface of the tubes are at high risk of wear and abrasion. Therefore, a material with high wear resistance has to be selected for this part. Tungsten Carbide is one of the best options for protection against extreme wear and impact as it is one of the hardest materials available. It is already used in industry for wear resistance applications such as coating, nozzles, ball valves, seal rings etc [22]

Tungsten carbide has a greater compressive strength rather than tensile strength. Usually tungsten carbide refers to a sintered composite of tungsten carbide grains embedded in and metallurgically bonded to a ductile matrix, or binder phase. Binders increase the tensile strength and support tungsten carbide grains. Decreasing the size of the tungsten carbide particles. Decreasing the size of the tungsten particles and reducing binder content increases the hardness, compressive strength and wear resistance. Considering that tungsten carbide is already used for nozzles which are impacted by the abrasive particles at a sharper angle, and its high wear resistance properties, it is a good candidate for the material of the tube. The following graph illustrates the variation of toughness, hardness and wear resistance of tungsten carbide [23].

Figure 13 :hardness, toughness and wear resistance of tungsten carbide.



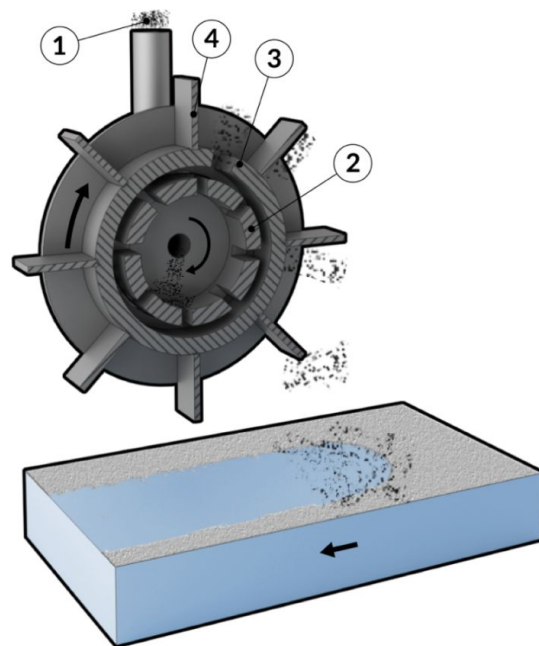
6.1.8. Material for masking the system

The system is at high risk of wear and abrasion by the abrasive particle. Therefore, rubber tapes are used in order to protect the whole system. The primary reason for this choice is that rubber absorbs the impact of the particle and forces it to bounce off with a considerably lower velocity which will prevent other possible damages. Also, there are abrasion resistant rubbers that are suitable for this task. There is an international standard instrument for measuring the hardness of a rubber and it is called durometer. Durometers measure hardness by the penetration of an indenter into the rubber sample. The calibrated reading is expressed in a number value. Considering the desired hardness and wear resistance that the rubber must provide the durometer is chosen. A rubber tape with hardness of 80A to 95A is used for abrasive applications due to longevity of the material and therefore is suitable for this task [24].

6.2. Blaster

In order for the machining to occur in a vacuum or low-pressure environment, traditional air jet machining cannot be used, since this would introduce high-pressure air into the environment. As such, alternative methods of accelerating abrasive particles need to be explored. Shot blasting is a process used currently to clean and strengthen metals by propelling abrasive material without using air. Wheel blasting is a type of shot blasting which uses rotating turbine wheels to propel abrasive material in custom blast rooms designed to efficiently derust, clean, orpeen the surface of large metal objects. Although this solution is applied on a much larger scale than our project, we can use the same principles of centrifugal force to accelerate the abrasive material.

Figure 14: Wheel blasting diagram [25]



 MANUFACTURINGGUIDE

6.3 Speed Requirement

The main consideration for speed requirements was found in [2], in this paper a calculation is given for the kinetic energy needed for cutting brittle materials. The equation is given below for convenience. By knowing the kinetic energy and the mass of the particle, the speed can be found by the general kinetic energy formula for point masses [26].

$$E_{kin} = (C_{\delta V} E^{3/2} K_{IC}^6)/H^{13/2} \quad \text{Eq: 1}$$

$$E_{kin} = \frac{1}{2} m v^2 \quad \text{Eq: 2}$$

The values for borosilicate AF45 glass were also obtained from [2], and placed in the table below. Note that the prefactor for crack threshold is the same for all brittle materials.

Table 6: Shows the values for finding the kinetic energy of AF 45 glass.

| | |
|---|----------------------------|
| Apparent threshold for lateral crack $C_{\delta V}$ | 2.3E4 |
| Modulus [E] | 66.1E9 Pa |
| Knoop Hardness [H] | 5.55E9 Pa |
| Fracture toughness [K_{IC}] | 0.84E6 Pa/m ^{1/2} |
| Specific Mass [ρ] | 2720 kg/m ³ |

By plugging these values in the equations, it was found that a speed of 267 m/s is required for the particles. The python program in Appendix A2, can be used to test this and also includes values for several other glasses for comparison. Minimum impact velocity for some other materials are also tabulated in the table below:

Table 7: Minimum impact velocity to cause lateral cracks

| | Velocity (m/s) | | | | |
|----------|---------------------|----------|-----------|-----------|-----------|
| | Particle Diameter | 5 micron | 10 micron | 15 micron | 20 micron |
| Material | Fused Silica | 1154 | 408 | 222 | 144 |
| | Spinel | 922 | 326 | 1774 | 115 |
| | Aluminum Oxynitride | 1721 | 608 | 331 | 2151 |
| | Sapphire | 3488 | 1233 | 671 | 4360 |

| | | | | | |
|--|---------------------|------|------|-----|-----|
| | Crystalline Alumina | 2345 | 829 | 451 | 293 |
| | Float Glass | 313 | 110 | 60 | 39 |
| | Glass Ceramic | 272 | 96 | 52 | 34 |
| | Quartz | 164 | 58 | 32 | 21 |
| | Pyrex | 2990 | 1057 | 575 | 374 |
| | Soda Lime | 393 | 139 | 75 | 49 |
| | Silicone Carbide | 2247 | 794 | 432 | 281 |
| | Borosilicate (A45) | 698 | 247 | 134 | 87 |

Table 8: Material Properties used for generating table 7

| Property | | | | | |
|----------|-------------------------|-----------------|-----------------------|--------------------------|----------------------|
| | | density (kg/m3) | elastic modulus (GPa) | fracture toughness (MPa) | Knoop hardness (GPa) |
| Material | Fused silica | 2210 | 70 | 0.78 | 4.5 |
| | Spinel | 3590 | 268.5 | 1.7 | 13.5 |
| | Aluminium oxynitride | 3690 | 324.5 | 2.4 | 16 |
| | Sapphire | 3970 | 365 | 3.25 | 17.5 |
| | polycrystalline alumina | 3986 | 390 | 3.5 | 21.5 |
| | Float glass | 2500 | 72 | 0.65 | 5.72 |
| | Glass ceramic | 2400 | 65 | 0.71 | 6.33 |
| | Quartz | 2650 | 76.5 | 0.7 | 7.57 |
| | Pyrex | 2520 | 460 | 0.75 | 5 |
| | soda lime | 2440 | 73.3 | 0.7 | 5.733 |
| | silicone carbide | 3200 | 130 | 5 | 23.5 |
| | borosilicate | 2720 | 66.1 | 0.84 | 5.55 |

6.4. Feeder

The purpose of the feeder apparatus is to extract abrasive material as needed, while controlling the flow rate into the blaster. The abrasive material will be extremely small, so the movement of the particles must be at a consistent rate to prevent clumping and clogging. There are many solutions to moving a solid material in powder form, and these designs are applicable to the small abrasive used in this project. Initially, we looked into using positive displacement pumps, which translate rotational force into the linear movement of a liquid or powder in a tube. Screw pumps, lobe pumps, and vane pumps are generally used to transfer slurries in a tube, but they require a pressure difference to generate suction.

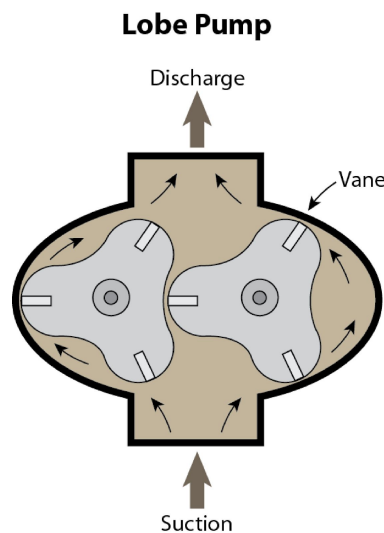


Figure 15: Lobe Pump Diagram [27]

Figure 15 illustrates the particle movement and the expanding volume suction created by the rotation in a lobe pump.

Screw conveyors, sometimes referred to as augers, are a very simple mechanism designed to move solids along a tube, very commonly seen in farming equipment to transport grains and powders. There are many difficulties with transporting micron-sized abrasive particles, but all can be overcome with a well-designed screw conveyor.



Figure 16: Centercore Auger [28]

Firstly, the micron-sized abrasive particles are a fluid powder. This means that round wire screws will not be able to efficiently move the material [28]. A centercore auger, as shown in Figure 7, will be able to better handle the small size powder and prevent it from sliding back. Augers with flat flight surfaces are suitable for powders much smaller than necessary for this project, such as fumed silica, which is only 0.2 to 0.3 microns in diameter [29]. These flat-wire screws will also minimize radial force, reducing the wear on the conveyor wall from the abrasive material. There are no internal bearings, and the screw is the only moving part in contact with the particles, so wear will be minimal and maintenance will be simple [29]. As mentioned earlier, another problem with the tiny abrasive particles is binding due to humidity. Augers are able to operate in a sealed tube, and as such will not introduce more air into the system.



Figure 17: Flat wire, beveled wire, square bar, and round wire screw profiles [28]

6.5. Enclosure

When dealing with any vacuum chamber it is key to note what pressure the use case needs to achieve. The problem is that the lower your pressure the harder it is to keep it at that pressure and the more important material and design considerations become. An example of how complex these considerations can be is given in [30]. In this section we will go over the research and calculations done to model the drag of the abrasive material, which in turn dictates the pressure needed. With the pressure known, we go over the material and design considerations appropriate for the pressure level and if purchasing an enclosure is a viable situation.

6.5.1. Pressure Requirement & Modeling of Particle speed in air

Since the design has not been finalized yet, the calculations done here only look at the particle dynamics after leaving the nozzle and before hitting the glass. The main consideration in terms of the pressure needed, is the drag force acting on the particles. Drag force greatly affects the speed of the particles as they leave the nozzle because of their small mass. As was explained before the material to be machined is AF 45 borosilicate glass, and it needs to hit the glass surface at 267 m/s. In order to ensure this speed is achieved when the abrasives hit the material surface, we calculate how much the particles will lose speed from drag at different pressures.

The drag force on the abrasive was calculated using the suggested method in [31] for flow past immersed bodies. The fluid being the air surrounding the particles. From there we need to first identify the type of flow present, and the Reynolds number is calculated to do this.

$$Re = \frac{\rho UL}{\mu} \text{ (Eq: 3)}$$

ρ = *air density at pressure P*

U = *air velocity (use particle velocity)*

L = *perpendicular to flow length of particle*

μ = *viscosity of air*

The Reynolds number, U parameter is meant for the flow velocity, however we don't know what this will be and we are assuming that the particles are going to follow the streamline of the flow as was mentioned in the theory section. This is why the use of velocity of particles is seen as appropriate. It should be noted that the Reynolds number is needed because of the dependence of the coefficient of drag C_d , on the type of flow as well.

When the type of flow is determined It is needed to now find the drag force $F_d(C_d, \rho, U, A_{wet})$.

The drag coefficient can be found from tables [31] or calculated as was done in [10]. In any case

the Drag coefficient of the abrasives is 0.86, as they are modeled as spheres. A_{wet} is the cross sectional area of the particle when facing the flow. In the case of a sphere it is just the area of the circle inscribed in the sphere.

$$F_d = C_D \frac{\rho}{2} U^2 A_{wet}$$

Assuming the particles have no other significant forces acting on them, the Force can be used to find the particles' deceleration and then the speed using the equations of projectile motion [26]. For simplicity the simplified final equation for velocity is given.

$$U_{final} = \sqrt{U_{initial}^2 + 2 a \Delta d} \quad , \quad a = F_d / m$$

$a = \text{acceleration}$
 $m = \text{mass}$
 $\Delta d = \text{change in position}$

Δd is considered to be 0.08m, as the distance between the nozzle and workpiece. The value of 8 cm is considered to be a worst case scenario. From these equations a Matlab program and database was made to easily calculate the resulting speed values at different pressures (in bar). The results are shown in table S1T, and the code is in Appendix A1.

Table 9: Assumes an initial launch at 275 m/s, the resulting speed is tabulated below.

| Pressure (bar) | Resulting Speed (m/s) |
|-------------------|-----------------------|
| 1.12 (atmosphere) | 63 |
| 0.02 | 271 |
| 0.01 | 273 |

It should be noted that the values for resulting speed should be calculated recursively, as the drag force is reduced with reduced speed.

With this calculation we determined that anywhere between 0.02 and 0.01 bar of pressure is needed to make the effects of drag negligible.

6.5.2. Device Selection

While noting that the pressure needed to achieve is (0.01~0.02) bar, and the fact that the system in general will most likely require some sort of shaft access through the vacuum chamber wall. We look at different possible options commercially, and try and estimate if building / modifying is a viable option.

Since the needed vacuum pressure is quite high compared to what is available in the market, there is no issue in finding a chamber. The main question then comes down to price and how

easily modifications can be made to meet our requirements. Currently we have requested a quote from lacotech for their series VI[33] vacuum chambers, they offer special requests such as extra ports and modifications. Mainly the vacuum chamber will need an access port for the shafts of all the moving parts, and also be lined with abrasive resistant material. Depending on price, and the attainable pressure that we require, it is also possible to design ourselves.

6. Requirements

After consulting with the professor certain, requirements have been modified. Here we have listed them by category. It should be noted that we have also added some requirements for human factors consideration which are appropriate for a lab environment .

1. Functionality

- a. Must provide the abrasives with necessary kinetic energy to cause radial fracture in the substrate
 - i. 247 m/s in the case of aluminum-oxide as abrasive and silicate glass A45 as substrate
- b. Features achieving width to depth ratio of 1:1 or above
 - i. Width current AJM processes, achieving 1:1 ratio results in a v-shaped cross section which is highly undesirable [2]
- c. The maximum trace of the impinging jet must be less than 12 mm^2
- d. Have a user interface
 - i. The user interface should include an emergency shut off
 - ii. Be appropriate for a shop/lab environment where gloves will be worn.
 1. The use interface relies on mechanical input from the user, however, not limited to only mechanical input.
 - iii. Allow for start / stop functionality
 - iv. Allow for feedback in terms of time remaining, flow rate and other important characteristics.
 - v. Users must be able to control the flow rate of abrasive etching the part.
 1. If the flow rate exceeds its threshold, it would increase the particle interactions with one another and result in obstruction of flow [1]
- e. Operator must be able to change the standoff distance of the nozzle from the sample
- f. The impact angle can be changed
 - i. In the range of $\pm 90^\circ$
- g. Allow visibility of work piece.
 - i. Visibility does not need to be direct or even at a straight angle
 - ii. Should at minimum allow for identifying emergency situations, such as malfunctioning components or fire hazards.
- h. Use electricity as energy input

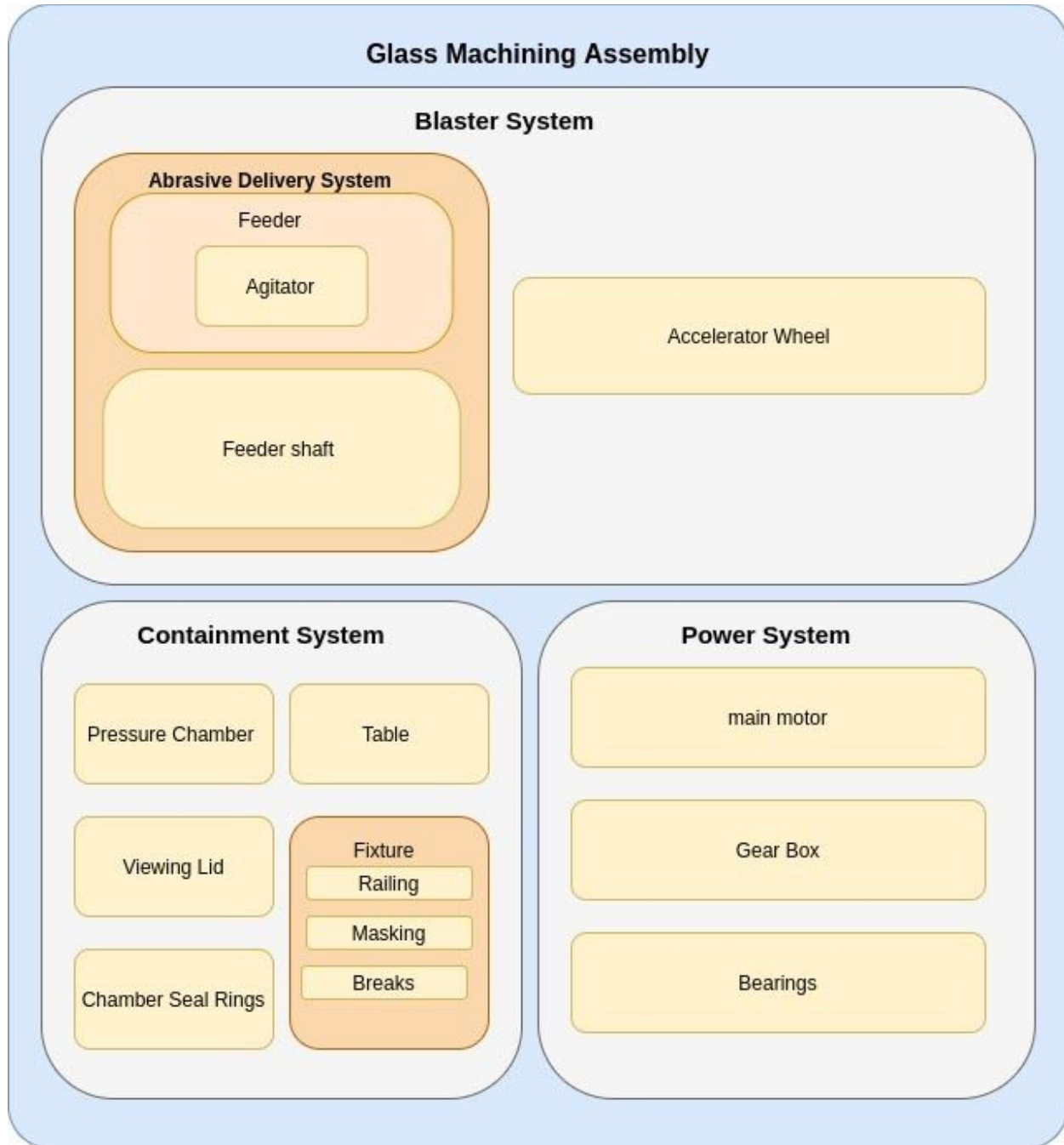
2. Maintainability

- a. Be large enough to allow easy access and maintenance

- i. Approximate size of 1 m^3
 - b. The leftover abrasives must be cleaned and vacuumed
 - c. Abrasion resistant parts of the enclosure can be replaced at a regular basis
- 3. Human Factors
 - a. User must be able to Load/unload Samples
 - b. Easy access for maintenance parts
 - i. Any Abrasive resistant lining should be easy to change
 - ii. All shafts, and wire ports should allow for removal of that shaft or wire.
 - c. The chamber must be enclosed so abrasive would be vacuumed before entering the air

7. Systems

Figure 18: Diagram of all systems and designed components.



Legend:



The system diagram in figure 16, summarizes the systems in our assembly and also shows exactly what major components were under our design consideration. It should be noted however that the shaft is only mentioned under the abrasive delivery system but the shaft was actually one of the main focuses of design and was interacting with all the systems. For better explanation we have included a listing and description of all the parts seen in figure 16. This is not an exhaustive list of all components (that can be seen in appendix X with the bill of materials). This listing describes the custom parts and main components used in the design for easier identification and purchasing.

7.1 Major Component Listing

7.1.1 Blaster System

The feeder includes two main parts, the upper and lower chambers. The upper chamber houses the overflow of the actual abrasive with an agitator within it that moves with the shaft. The lower chamber includes a screw that pushes the abrasive forward into the main hollow shaft and then through the particle accelerator.

The feeder mechanism was designed to meet two main requirements, first as a way of storing the abrasive without it clumping together like wet sand. The second was to control the feed rate of the abrasive and have a way of it acting as a valve. In our design if the screw stops turning the abrasive will no longer flow through to the accelerator wheel. This will limit how much abrasive is wasted as the abrasive cannot be reused.

The accelerator wheel is the most important and simple part of the Blaster system. It acts as part of the main shaft and is used to guide and accelerate the particles of abrasive to the glass samples. The radius and number of spokes on the wheel were designed to allow for correct exit speed and max flow rate of abrasive.

Table 10: Blaster Component listing.

| Component | Listing |
|---|-----------------------------|
| All components are custom made for Blaster sys. | See appendix X for drawings |

7.1.2 Containment System

The containment system includes the main enclosure and structural components. The system is lined with abrasive resistant rubber where in contact with abrasive. The main chamber holds a fixture on its walls. The fixtures are locked in place on the walls of the chamber. The fixture is

used to hold the glass samples and allows for minor position adjustment to get the samples in the way of the abrasive path for best cutting.

The system includes a view window made of acrylic supplied as a unit with the chamber by LACO technologies. This allows for the user to see if the abrasive is contacting the samples best.

The chamber also is placed onto a custom table. The table locks the chamber onto itself with two screw tightened belts. The table allows for the user to use the device at an ergonomic height and also have space for mounting the motor underneath the table.

Table 11: Containment system Component listing.

| Component | Listing |
|----------------|---------------------------|
| Vacuum chamber | LACO Tech. VI series [33] |

7.1.3 Power System

The power system includes the most expensive parts of the design. The complexity and importance of these components require mass production components to be used for the design. Further these components usually require further support through their life, and various warranties will help keep the users investment well spent.

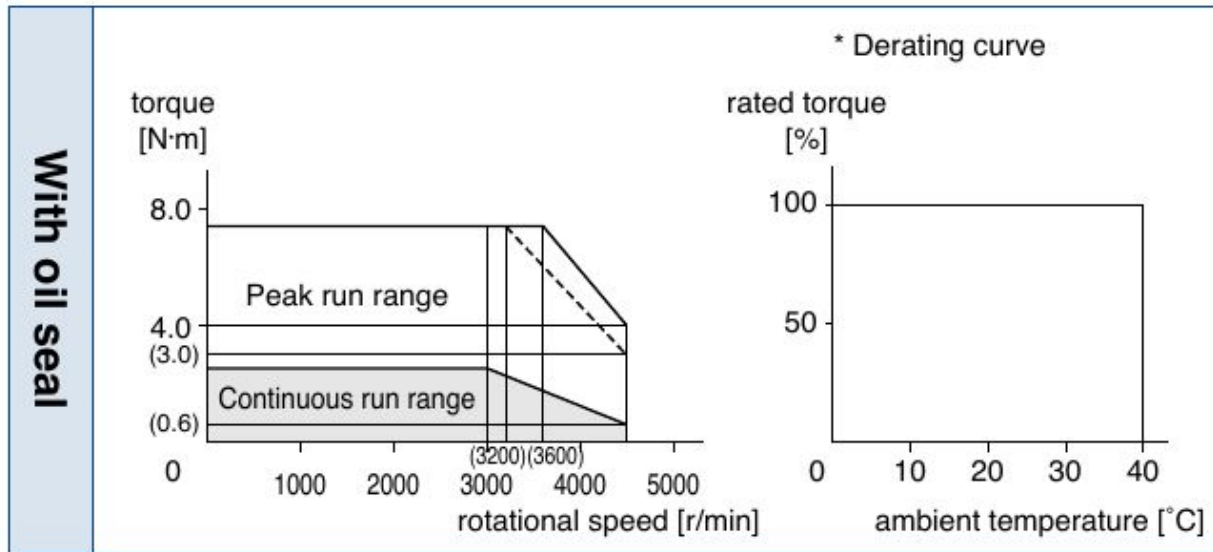
The motor is the MSMD082S1U motor from supplier digi key. The motor can supply the needed torque with more than enough headroom (2.4 Nm). The motor can run upto 3200 RPM without significant loss of torque from the 2.4 Nm range. Since before the gear box we only need 1.4 Nm of torque this means that there is room for error in our calculations for adjusting the needed speed and torque. The motor requires 200V input which means regular mains power will not be suitable but comes with its own dedicated driver.

The motor has a constant torque speed curve upto 3000 RPM and does not lose much till 3200 RPM as can be seen in figure 20. Given the recommendations of the manufacturer the motor is best kept in the blue region of the figure 20. This means that the RPM should be about 3000 RPM which can then be stepped up to 12000 RPM with the gear box. This is again enough for our needs.

Figure 19. Shows the MSMD082S1U motor used in the design.



Figure 20. The torque speed curve of the MSMD082S1U motor. [34]



The motor image can be seen in figure 19 and has a price tag of \$1300 per unit. The shaft diameter itself is also 17.5mm and is suitable for our design with a keyway placed in for power transmission.

It should also be noted that this is a high resolution servo motor and considering that is one of the most expensive components of the setup the user can easily implement the motor for a variety of other applications and potentially reduce their cost basis from this.

The Gear box is The ATEX GXA series allows for 5:1 gearing in a step up and down setup. The image can be seen in Figure 21. The gear box is being used at the limits of its specs but the manufacturer does not specify any limitations on how long the gearbox can be in this state.

Figure 21: Shows the ATEX GXA series gearbox. [35]



For bearing the design needs to use specialized sealed bearings allowing keeping the vacuum seal while keeping the motor outside the chamber. This had to be done as the motor required cooling and sealing a shaft was seen as easier than sealing around wiring that could potentially be pulled out. For this purpose the 2 face seal NS-DF-2 variable diameter bearing is used from new air bearings. Figure 22 shows an image of this bearing.

Figure 22. Shows the NS-DF-2 Sealed bearing. This bearing can be adjusted between 25 and 51 mm. [36]



Table 12: Power System Component listing.

| Component | Listing |
|----------------|-----------------|
| Motor | MSMD082S1U |
| Sealed Bearing | NS-DF-2 |
| Gear Box | ATEX GXA series |

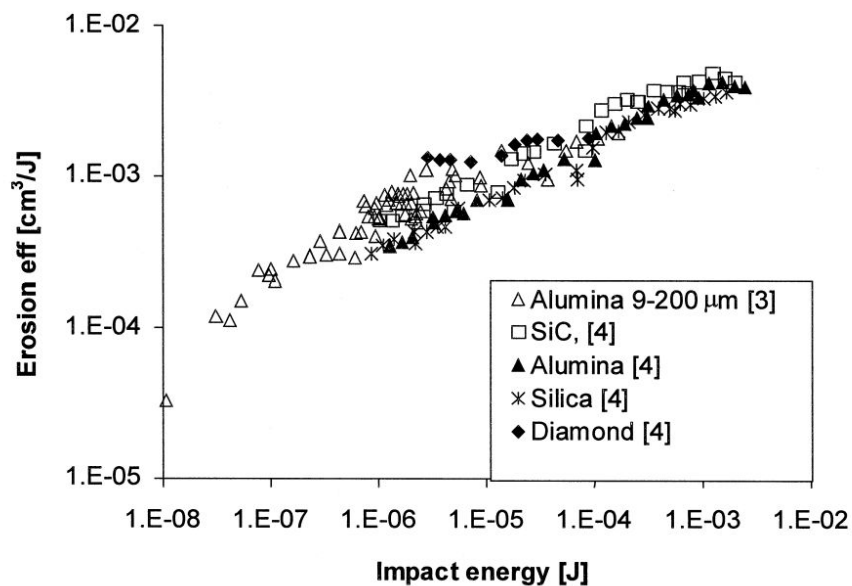
8. Detailed Design

8.1. Sample calculations:

Prediction of required abrasive mass flow rate:

Erosion rate or the rate of material removal is one of the deciding factors for prediction of mass flow rate of abrasive needed. The erosion rate is expressed as the ratio of removed material weight and the weight of impacting particles. According to Slikkerveer [37], **Kinetic energy** of the particles is the primary process parameter for erosion. To show this, they defined a new variable called Erosion **Efficiency** which is defined as the amount of substrate material(volume) removed pre amount of (kinetic) energy in the incoming particles $[\frac{cm^3}{J}]$. Figure 23 shows the erosion efficiency of Boro-Silicate glass (A45) as a function of kinetic energy of individual particles. The tests were conducted over wide ranges of particle sizes (9 – 200 μm) and velocities (30-250 m/s) and number of erodent materials varying from silica to diamond. Their findings are particularly important as it shows that the erosion efficiency is independent of abrasive media and the same erosion process [erosion efficiency] can be achieved by erodent of any size, as long as the impact velocity is adjusted to achieve the same kinetic energy.

Figure [23]: The erosion efficiency of glass plotted against the kinetic energy of the individual particle for a wide range of erodent sizes, velocities and a range of erodent materials [extracted from M2]



Based on the previous analysis for the minimum impact velocity based on the minimum kinetic energy needed to cause lateral cracks, the minimum energy is $U_{kin} = 6.3 \times 10^{-8}$, and for ($10\mu m$) particles, it corresponds to a minimum speed of 270 m/s. Using Figure 23, it can be found that the erosion efficiency of the powder blasting process is of the order of $10^{-3} \frac{cm^3}{J}$, and follows the fitted equation of the following[37]:

$$E_{eff} = 9 \times (\text{impact energy}) + 9.91 \times 10^{-5} \quad (\text{Eq: 4})$$

Using the minimum kinetic energy required, the erosion efficiency yields to be $8.5 \times 10^{-5} \frac{cm^3}{J}$. Assuming that the eroded surface is a channel with aspect ratio of 1:1 (width:depth), the overall energy required for for eroding 1cm (in length) of the channel can be calculated as:

$$\text{Energy required} = 1.176 \times 10^4 [E_{eff}] \times (\text{width of channel})^2 \quad (\text{Eq: 5})$$

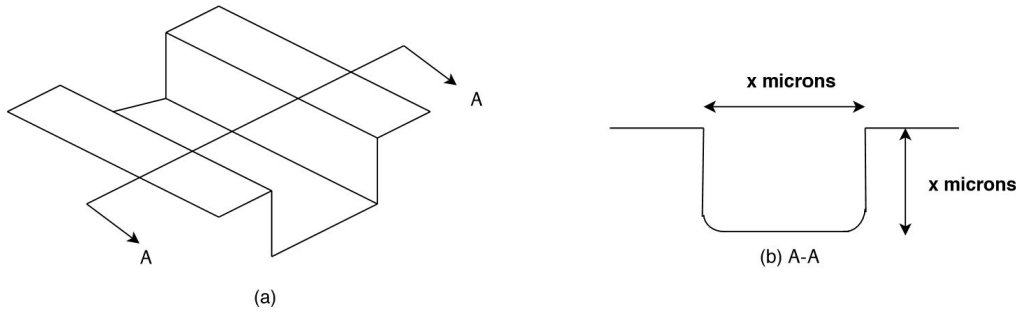


Figure 24: a)schematic of the channels and b) cross-sectional area of the erodant channel.

Assuming velocity of $270 \frac{m}{s}$ for the impacting particles, the required mass per 1cm of the channel as a function of width of channel is:

$$\text{Mass needed } (\frac{gr}{cm}) = \frac{2 \times \text{Energy required}}{V^2} = 9.191 \times 10^2 \times (\text{width of channel})^2 \quad (\text{EQ: 6})$$

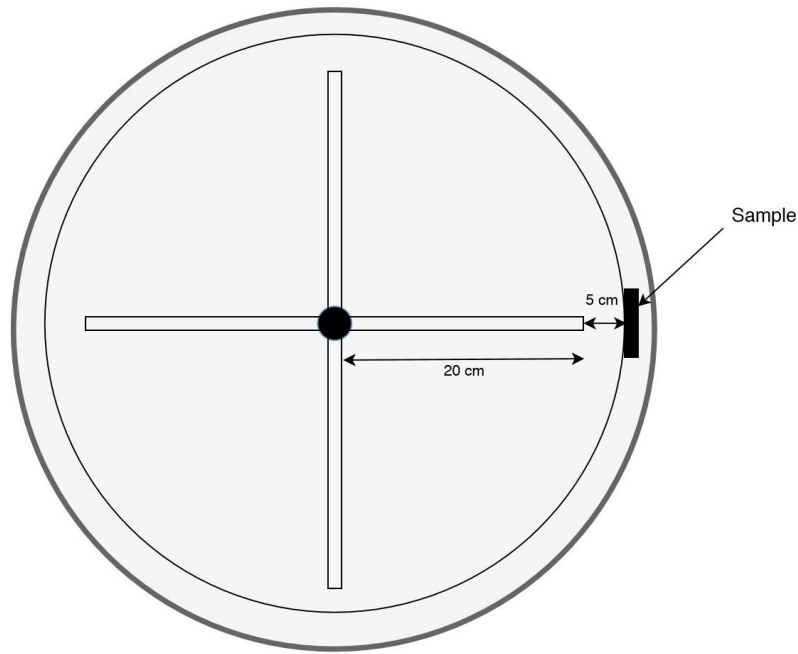
Based on the 20cm radius of the blasting wheel and 5cm stand-off distance between the sample and the wheel, the samples are placed on a 25cm radius from the centre of the chamber[refer to figure 25]. Since the blaster is running continuously, the blaster should provide a flow at the specified rate for the whole perimeter of the 25cm-radius circle that the samples are placed on.

$$\text{Circles}_{perimeter} = 2\pi r = 157.08 \text{ cm} \quad (\text{Eq: 7})$$

=> overall mass needed per width of channel=

$$\text{Mass needed } \left(\frac{\text{gr}}{\text{cm}}\right) \times \text{Circles}_{\text{perimeter}} = 1.44 \times 10^5 \times (\text{width of channel})^2 \quad (\text{Eq 8})$$

Figure 25: Top view of the chamber, showing the position of the samples with regard to the centre of the chamber.

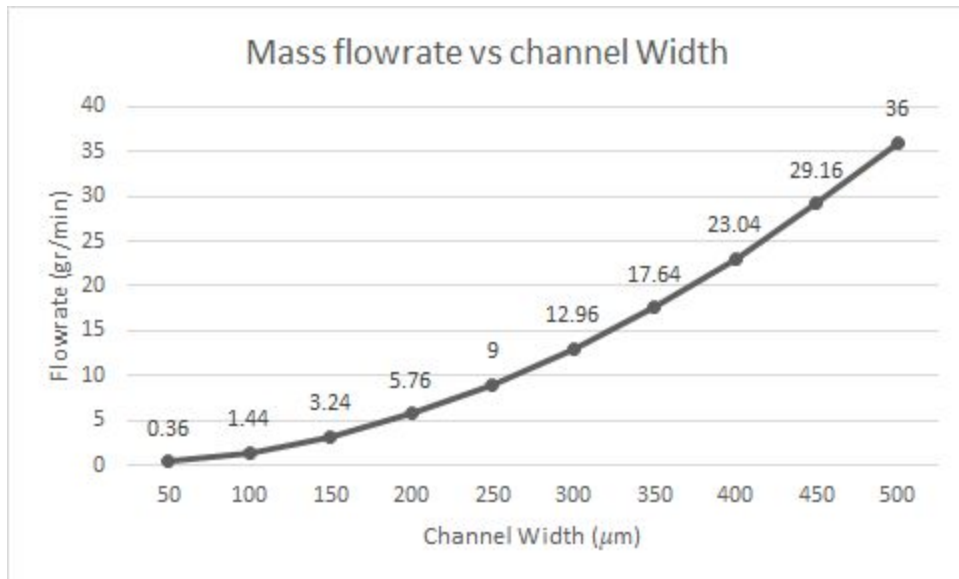


Assuming the process should be done in less than 10 minutes, the overall mass needed based on different ranges of width of the channel is tabulated in the following table.

Table 13: Mass flow rate needed in (gr/min) for variety of channel width, assuming the process must be over in less than 10 minutes.

| Channel Width (μm) | 50 | 100 | 150 | 200 | 250 | 300 | 350 | 400 | 450 | 500 |
|---------------------------------|------|------|------|------|-----|-------|-------|-------|-------|-----|
| Mass flow rate (g/min) | 0.36 | 1.44 | 3.24 | 5.76 | 9 | 12.96 | 17.64 | 23.04 | 29.16 | 36 |

Figure 26: Mass flowrate versus channel width (Aspect ratio of 1:1)



Calculating speed and angle of particles shooting out of the blaster wheel:

Figure 27: schematic of the particle and its corresponding velocity as it travels in the tube

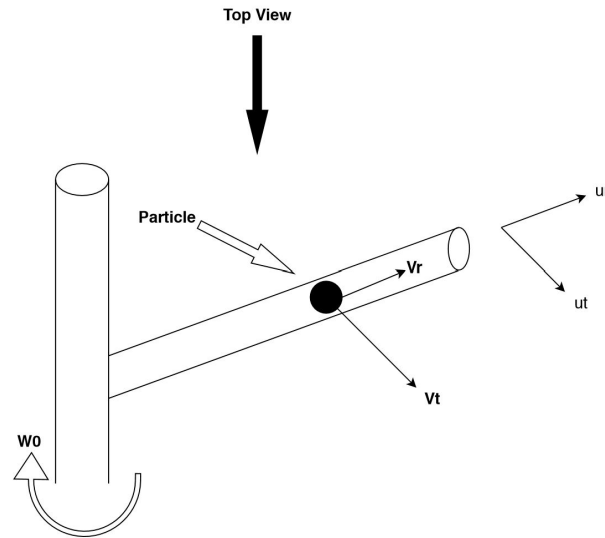
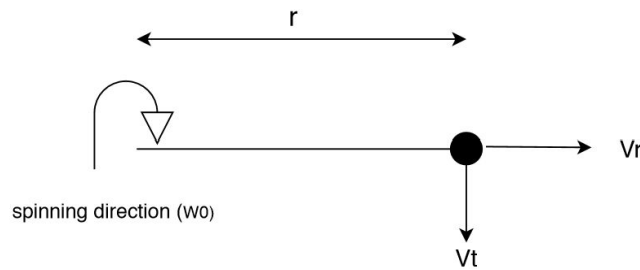


Figure 28: Top view of the schematic showing position of the particle



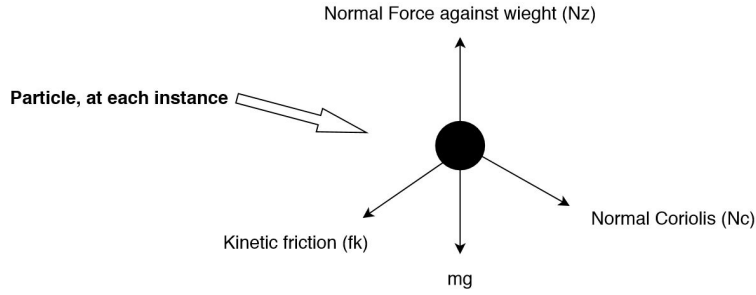
* r shows the position of the particle with respect to the centre of the blaster wheel.

Assumptions:

- Since the angular velocity is kept constant, the normal force is a combination of normal force caused by coriolis acceleration (N_c) and normal force opposing weight of particles.
- Kinetic friction is dependent on normal force.
- Since the particles are irregular in shape, no rotation is considered for them as they travel down the tube.
- The interaction of particles is not assumed in this analysis.

e) The tangential speed of the particle exiting the tube is assumed as the particle is spinning at the tip of the tube.

Figure 29: FBD diagram of the particle and the forces acting on the particle



$$1) a^{Coriolis} = 2.r'.\omega \Rightarrow N_c = a^{Coriolis} . m = 2.r'.\omega . m \quad (\text{Eq: 8})$$

- ❑ Where $a^{Coriolis}$ is coriolis acceleration induced by radial velocity of particles and angular velocity of the tube.
- ❑ $Vr = r'$ is the radial velocity of the particle travelling down the tube. ω is the angular velocity of the tube.
- ❑ m is the mass of the particle.
- ❑ N_c is the normal force induced by the coriolis acceleration.

$$2) N_{total} = \sqrt{N_c + N_z} = \sqrt{(2.r'.\omega . m)^2 + (mg)^2} \quad (\text{Eq: 9})$$

- ❑ Where N_z is the normal force opposing weight of the particle.

$$3) f_k = N_{total} . \mu_k == \sqrt{(2.r'.\omega . m)^2 + (mg)^2} . \mu_k \quad (\text{Eq: 10})$$

$$\Rightarrow a_{fk} = \sqrt{(2.r'.\omega)^2 + (g)^2} . \mu_k$$

- ❑ Where f_k is the kinetic friction acting on the particle travelling down the tube.
- ❑ μ_k is the coefficient of kinetic friction. It is assumed as smooth contact with $\mu_k < 0.2$.

$$4) a_{centrifugal} = r.\omega^2 \quad (\text{Eq: 11})$$

- ❑ Where $a_{centrifugal}$ is centrifugal acceleration of the particle along \underline{ur} .

$$5) a_{radial} = a_{centrifugal} - a_{fk} = r.\omega^2 - 2.r'.\omega. \mu_k \quad (\text{Eq: 12})$$

□ a_{radial} is the radial acceleration of the particle along ur .

$$6) V_{tangential} = r. \omega \quad [\text{assumption e}] \quad (\text{Eq: 13})$$

7) $V_{radial} =$ to calculate the radial velocity, a matlab code was developed that would iteratively calculate the speed of the particle as it is travelling through the tube. As the particle gets farther from the centre, the normal force and as a result, its radial acceleration changes. At each iteration, the instantaneous radial acceleration is calculated and it updates the Vr. For the iteration, the following equation was used:

$$8) r_2'^2 = r_1'^2 + 2.a_r.(\Delta d) \quad (\text{Eq: 13})$$

For which, the $\Delta d = 1mm$ is the incremental distance for each iteration.

Table 14: Radial speed, Total speed, and departure angle based on different coefficient of friction at 9500 RPM.

| Iteration | 1 | 2 | 3 | 4 | 5 |
|---|--------|--------|--------|--------|--------|
| Wheel speed (RPM) | 9,500 | 9,500 | 9,500 | 9,500 | 9,500 |
| Coefficient of Kinetic friction (μ_k) | 0.00 | 0.05 | 0.10 | 0.15 | 0.20 |
| Tangential Velocity (m/s) | 198.97 | 198.97 | 198.97 | 198.97 | 198.97 |
| Radial Velocity (m/s) | 198.43 | 188.81 | 179.68 | 171.02 | 162.84 |
| Departing Angle (Degrees) | 44.92 | 43.50 | 42.08 | 40.68 | 39.30 |
| Total Velocity (m/s) | 281.00 | 274.30 | 268.09 | 262.37 | 257.11 |

Based on the Results tabulated in table 11, it is shown that at each instance, the particles leave the wheel with $\approx 40^\circ$ angle with respect to the line tangent to the blaster wheel. However, based on the Coefficient of Kinetic friction, this angle can vary by $\approx 5^\circ$. To ensure that the particles can impact the target at perpendicular angle, the fixtures holding the samples can be calibrated to accommodate that.

Figure 29: the Matlab code used to iteratively calculate radial velocity of the particle

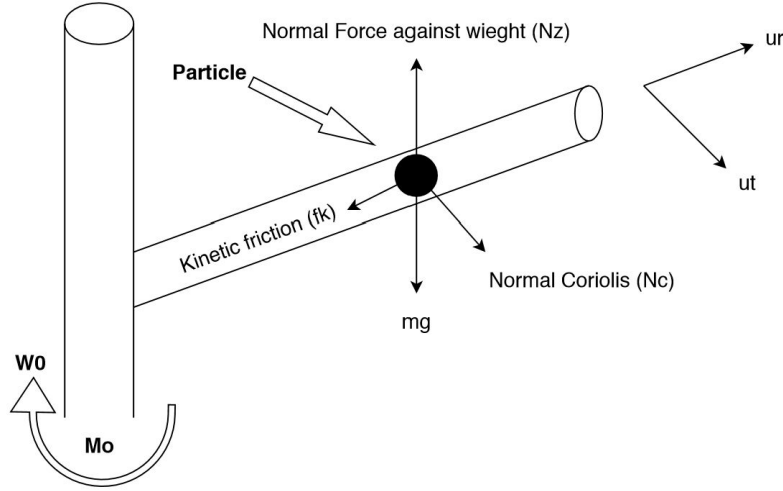
```
clear all;

sl= 0.2;           %shaft length
g= 9.81;           %gravitational force
f_coef=0.15;       % coeffecient of kinetic friction
v0=sqrt(g*sl*2);   %speed entering the wheel
r0=0.005;          % in m, initial radius (starting)
rf= 0.2;           % in m, radius of the wheel
spacing=0.001;     % delta d = 1mm
r=(r0):spacing:(rf-0.001); % array for iteration
vr=[];             % velocity array
ar=[];             % acceleration array
vr(1)=v0;          %initial radial velocity (m/s)
w_rpm= 9500;       % angular velocity in rpm
w=w_rpm*2*pi()/60; %angular velocity in rad/s

for i=1:length(r)
    ar(i)=r(i)*w^2-2*w*vr(i)*f_coef;
    vr(i+1)=sqrt(vr(i)^2+2*ar(i)*spacing);
end
vr_final=vr(length(vr)); % final radial velocity
vt=rf*w;                 % final tangential velocity
v_total=sqrt(vr_final^2+vt^2); % total velocity
angle_rad=atan(vr_final/vt);
angle_deg=rad2deg(angle_rad); % shooting angle
```

Calculating required torque to maintain the wheel speed

Figure 30: schematic of the particle and the corresponding forces acting on it



As the particles enter and travel along the tube, the forces acting on the particle cause them to accelerate in radial and tangential direction till they achieve their final required velocity. Considering the law of conservation of energy, the amount of energy transferred to the particles should correspond to the energy put into the shaft.

$$E_{in} = E_{out} \quad (\text{Eq: 14})$$

Assuming that the angular velocity of the shaft and tubes are held constant at 9500 rpm, the input energy can be calculated as following:

$$E_{in} = \text{Torque} \times \omega \quad (\text{Eq: 15})$$

Also, the energy transferred to the particles can be calculated as:

$$E_{out} = \frac{\dot{m}}{2} \times V^2 \quad (\text{Eq: 16})$$

From previous sections, the required terminal velocity of particles exiting the tube was calculated to be $270 \frac{m}{s}$ and the maximum flow rate to be $36 \frac{gr}{min}$. combining (X) and (Y), the required Torque can be calculated as following:

$$Torque = \frac{\dot{m} \times V^2}{2 \times \omega} = \frac{(36 \frac{gr}{min} \times \frac{1 min}{60 sec} \times \frac{1 kg}{1000 gr}) \times (270)^2}{2 \times (9500 rpm \times \frac{2\pi}{60})} = 0.022 N.m \quad (Eq: 15)$$

Assuming standard 15% torque loss at the bearings at high speeds, the required torque increase to $(0.026 N.m)$ which still is negligible.

Calculating Start-up torque

The goal for the start up period is that the rotating parts of the design reach the required speed in less than a minute. The rotating parts include the blaster wheel, input shaft, and the feeder shaft. For simplicity, some other components like the fastening bolts, keys, and retaining rings are ignored since their mass is negligible compared to other major parts. Since all the components are steel alloy, assuming density in the range of $[7.6-8] \frac{g}{cm^3}$, using the Solidworks built in “Mass Property evaluation”, the approximate moment of inertia for each component is listed in table 12:

Table 15: Moment of inertia of rotating components

| Component | I_{θ} = Mass moment of inertia about z-axis ($Kg.m^2$) |
|---------------|---|
| Blaster wheel | 0.01102 |
| Input shaft | 0.00458 |
| Feeder shaft | 0.00318 |
| Total | 0.01878 |

Given the system should reach the given speed in a minute, the required angular acceleration can be calculated as following:

$$Angular\ acceleration = \alpha = \frac{\Delta\omega}{\Delta t} = \frac{9500(RPM) \times \frac{2\pi(rad)}{60s}}{60\ sec} = 16.58 \frac{rad}{s^2} \quad (Eq: 16)$$

Given Angular acceleration, the required torque is calculated as:

$$Torque = \alpha \times I_{\theta} = 16.58 \times 0.01878 = 0.311\ N.m \quad (Eq: 17)$$

Given 15% torque loss at the bearings and joint, the required Torque is **0.366 N.m**.

Calculating the maximum moment applied on the shaft due to eccentricity

In this part, we assumed a worst case scenario of a clogged tube and 0.5% eccentricity of the weight of the disk. Using the volume of the tube and the density of the abrasive material the mass of the clogged tube was calculated:

$$m = v * \rho \quad (\text{Eq: 18})$$

Where:

m is the mass of the clogged tube (kg)

V is the volume of the tube

ρ is the density of the abrasive material

$$m = 2.513 * 10^{-6} * 3219 = 8.089 * 10^{-3} \text{ kg} = 8.089 \text{ g}$$

Considering that the mass of the disk is 1kg, a 0.5% eccentricity is equal to 5 grams resulting in an overall mass of 13 grams. The centrifugal force that this mass applies on the canter is:

$$F = mr\hat{\theta}^2 \quad (\text{Eq: 19})$$

Where:

F is the centrifugal force (N)

m is the total unbalanced mass (kg)

r is the radius from the centre to where the mass is located (m)

$\hat{\theta}$ is the rotational speed of the disk (rad/s)

r is half of the radius of the wheel, 100 mm. The rotational speed is 9500 rpm.

$$F = 0.013 * 0.1 * \left(\frac{9500 * 2\pi}{60}\right)^2 = 1286.6 \text{ N}$$

This force will be divided between the upper and the lower shafts equally. The critical location of the upper shaft that has to be analysed is where the shaft joins the thicker shaft. The moment that the disk applies on that point is:

$$M_{max} = \frac{F}{2} * r \quad (\text{Eq: 20})$$

Where:

r is the distance from the disk to the critical point.

$$M_{max} = \frac{1286.6}{2} * 0.040 = 25.73 \text{ N.m} \quad (\text{Eq: 21})$$

Calculating the diameter of the shaft

Considering the possible eccentricity and clog of one of the tubes, the wheel will apply a moment on the shaft. The unbalanced mass will cause a centrifugal force that can possibly lead to fatigue failure. Therefore, fatigue failure analysis must be done in order to calculate the minimum shaft diameter that can bear the stress. For calculating the minimum diameter of the shaft, the 10th edition of Shigley's Mechanical Engineering Design was used [38].

Using DE-Goodman method:

$$\frac{1}{n} = \frac{16}{\pi d^3} \left\{ \frac{1}{S_e} [4(K_f M_a)^2 + 3(K_{fs} T_a)^2]^{1/2} + \frac{1}{S_{ut}} [4(K_f M_m)^2 + 3(K_{fs} T_m)^2]^{1/2} \right\} \quad (\text{Eq: 22})$$

Where: n is the factor of safety

d is the diameter of the shaft (m)

S_e is the modified endurance strength of the material (Pa)

K_f is fatigue stress concentration factor

M_a is the amplitude of the moment (N.m)

K_{fs} is fatigue stress concentration factor for shear stress

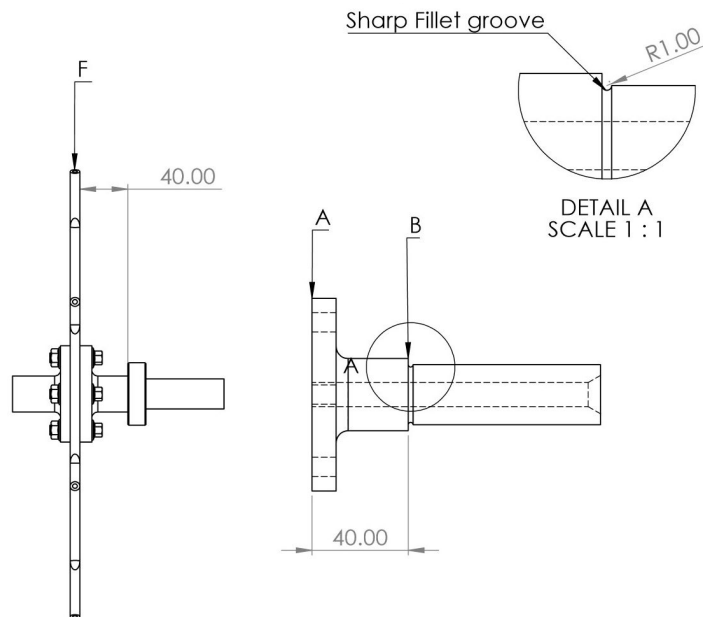
T_a is the amplitude of the torque (N.m)

S_{ut} is the ultimate tensile strength (Pa)

M_m is the midrange moment (N.m)

T_m is the midrange torque (N.m)

Figure 31: Schematic showing placement of the wheel and shafts



In our case, there is no torque and the bending moment is completely reversible meaning that the midrange moment is equal to zero. Therefore, simplifying and rearranging the above equation gives the following equation:

$$d = \left\{ \frac{16n}{\pi S_e} [4(K_f M_a)^2]^{0.5} \right\}^{\frac{1}{3}} \quad (\text{Eq: 23})$$

Finding S_e :

The material used for the shaft is cold-drawn AISI 1030 which has a S_{ut} equal to 520 Mpa.

$$S'_e = \begin{cases} 0.5S_{ut} & S_{ut} \leq 200 \text{ kpsi (1400 MPa)} \\ 100 \text{ kpsi} & S_{ut} > 200 \text{ kpsi} \\ 700 \text{ MPa} & S_{ut} > 1400 \text{ MPa} \end{cases}$$

Considering the S_{ut} of our material, it will have an endurance strength equal to:

$$S'_e = 0.5(520) = 260 \text{ MPa}$$

This value is unrealistic and depending on the material, manufacturing, environment and the design of the shaft, there are some modifying factors that are needed to be applied to the achieved value. The Marine equation, which is illustrated below, can be used to determine the value for the endurance strength that is closer to the real endurance strength of the shaft.

$$S_e = k_a k_b k_c k_d k_e k_f S'_e \quad (\text{Eq: 24})$$

where k_a = surface condition modification factor

k_b = size modification factor

k_c = load modification factor

k_d = temperature modification factor

k_e = reliability factor¹³

k_f = miscellaneous-effects modification factor

S'_e = rotary-beam test specimen endurance limit

S_e = endurance limit at the critical location of a machine part in the geometry and condition of use

Finding k_a :

The surface factor depends on the finishing of the shaft and its tensile strength.

$$k_a = aS_{ut}^b$$

Where a and b can be found from the following table:

| Surface Finish | Factor a | | Exponent b |
|------------------------|---------------|--------------|------------|
| | S_{ut} kpsi | S_{ut} MPa | |
| Ground | 1.34 | 1.58 | -0.085 |
| Machined or cold-drawn | 2.70 | 4.51 | -0.265 |
| Hot-rolled | 14.4 | 57.7 | -0.718 |
| As-forged | 39.9 | 272. | -0.995 |

Considering that our shaft has a cold-drawn finish and using the table above, it will result in a value of:

$$k_a = 0.85988$$

Finding k_b :

The size factor depends on the diameter of the shaft and can not be determined at this point, but once the diameter is achieved, the k_b has to be calculated and be replaced with the previous value and calculate the diameter again and do more iterations if it causes a significant difference in the diameter. To be able to continue the procedure, we will assume a value of 0.85. The true value has to be calculated using the following equation:

$$k_b = \begin{cases} (d/0.3)^{-0.107} = 0.879d^{-0.107} & 0.11 \leq d \leq 2 \text{ in} \\ 0.91d^{-0.157} & 2 < d \leq 10 \text{ in} \\ (d/7.62)^{-0.107} = 1.24d^{-0.107} & 2.79 \leq d \leq 51 \text{ mm} \\ 1.51d^{-0.157} & 51 < d \leq 254 \text{ mm} \end{cases}$$

These equations can be used for rotating shafts that are under bending or torsion.

Finding k_c :

Loading factor is only for the cases where the shaft is under axial or torsional loading and in our case is just equal to 1.

Finding k_d :

When the shafts are operating below room temperatures or very high temperatures, their strength might be affected. A low temperature might cause brittle fracture and a high temperature might cause yield failure as the yield strength has an inverse relation with temperature. From the available data it can be seen that the temperature starts impacting the endurance limit after 400F.

However, in our system the temperature is not going to reach that level and therefore, a temperature factor equal to 1 can be considered.

Finding k_e :

The reliability factor accounts for the scatter of data.

$$k_e = 1 - 0.08 z_a$$

The above equation is used to find the reliability factor. Choosing a reliability equal to 90%, the transformation variate, z_a , is going to be equal to 1.288 resulting in a reliability factor of 0.89696.

By computing the value of S'_e and the Marine modifying factors into eq(24), results in an endurance limit of:

$$S_e = 170.4516 \text{ Mpa}$$

Finding k_f :

On the locations that there exists a discontinuity such as holes, grooves or notches, the theoretical stresses increase significantly. Stress concentration factor counts in this impact.

$$K_f = 1 + q(K_t - 1) \quad (\text{Eq: 25})$$

The equation above is used to calculate k_f .

Finding q:

$$q = \frac{1}{1 + \frac{\sqrt{a}}{\sqrt{r}}} \quad \text{Where: } \sqrt{a} = 0.246 - 3.08(10^{-3})S_{ut} + 1.51(10^{-5})S_{ut}^2 - 2.67(10^{-8})S_{ut}^3$$

For bending or axial

This formula uses kpsi for the unit of the S_{ut} . Hence, computing the value of 76 kpsi into the equation results in:

$$q = 0.9196$$

Finding k_t :

The value of k_t depends on the diameter of the shaft and can not be determined at this point, but once the diameter is achieved, the k_t has to be achieved and be replaced with the previous value

and calculate the diameter again and do more iterations if it causes a significant difference in the diameter. To be able to continue the procedure, we will use the following table and assuming a shoulder fillet-well rounded, a value of 1.7 will be considered for k_t .

First Iteration Estimates for Stress-Concentration Factors K_t and K_{ts} .

Warning: These factors are only estimates for use when actual dimensions are not yet determined. Do *not* use these once actual dimensions are available.

| | Bending | Torsional | Axial |
|--|---------|-----------|-------|
| Shoulder fillet—sharp ($r/d = 0.02$) | 2.7 | 2.2 | 3.0 |
| Shoulder fillet—well rounded ($r/d = 0.1$) | 1.7 | 1.5 | 1.9 |
| End-mill keyseat ($r/d = 0.02$) | 2.14 | 3.0 | — |
| Sled runner keyseat | 1.7 | — | — |
| Retaining ring groove | 5.0 | 3.0 | 5.0 |

Computing the values of q and k_t into eq(25) results in:

$$k_f = 1.64372$$

Note that once the true value of k_t is found, k_f has to be modified as well.

Finding n : for this design, a safety factor of 3 was considered in order to find the diameter of the shaft.

Finding M_a :

The moment depends on the percentage of the eccentricity. As previously calculated, an eccentricity of 0.5%, causes a moment equal to 25.73 N.m. The formula for finding the amplitude of the moment is:

$$M_a = \frac{M_{max} - M_{min}}{2} = \frac{25.73 - (-25.73)}{2} = 25.73 \text{ N.m}$$

Finding d :

Now that all the variables in eq(22) have been found, substituting them into the formula results in:

$$d = 0.019646m$$

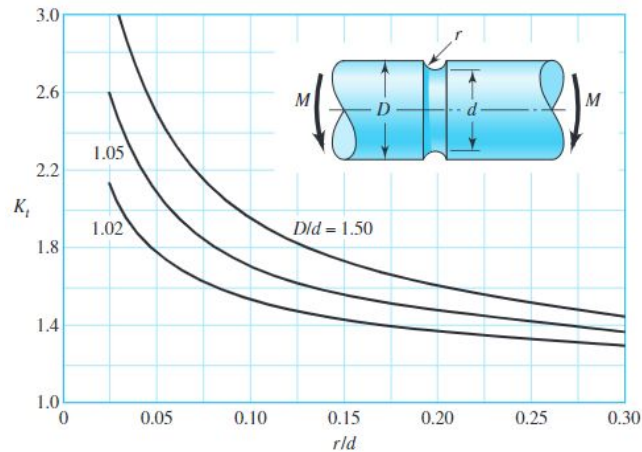
Calculating the true value of k_b :

$$k_b = 0.9017$$

finding the true value of k_t :

Using the following figure, $D=40\text{mm}$, $d=19.646\text{mm}$ and $r=1\text{mm}$:

$$k_t = 2.6$$



2nd iteration using the new values of k_b and k_t results in:
 $d = 0.02207\text{m}$

New values of k_b and k_t

$$k_b = 0.8905$$

$$k_t = 2.5$$

3rd iteration using the new values of k_b and k_t :
 $d = 0.02188\text{m}$

New values of k_b and k_t :

$$k_b = 0.8913$$

$$k_t = 2.5$$

As it can be observed, after the 3rd iteration, the values of k_b and k_t almost stay the same and have negligible differences in each iteration. Therefore, a value of $d = 0.02188\text{m}$ is acceptable for the minimum diameter of the shaft. However we have to note that this procedure is for solid shafts. As our shaft is hollow, the outer diameter of a hollow shaft that would be equivalent to the solid one can be found by the following formula:

$$d^2 = d_o^2 - d_i^2$$

Where:

d = diameter of the solid shaft

d_o = outer diameter of the hollow shaft

d_i = inner diameter of the hollow shaft

The inner diameter of the shaft is 10 mm. Therefore the minimum outer diameter of the hollow shaft that will not face fatigue failure for a safety factor of 3 and 0.5% eccentricity is:

$$d_o = 24.06 \text{ mm}$$

The outer diameter of the design is 25 mm ensuring the safety of the shaft.

The following table illustrates the minimum allowable outer diameter (mm) of a hollow shaft for different percentages of eccentricity for different materials in order of their ultimate tensile strength.

The materials are:

Cold-drawn AISI 1018 ($S_{ut} = 440 \text{ Mpa}$)

Cold-drawn AISI 1030 ($S_{ut} = 520 \text{ Mpa}$)

Cold-drawn AISI 1040 ($S_{ut} = 590 \text{ Mpa}$)

Table 16: The outer diameter of the hollow shaft(mm) based on the eccentricity and material.

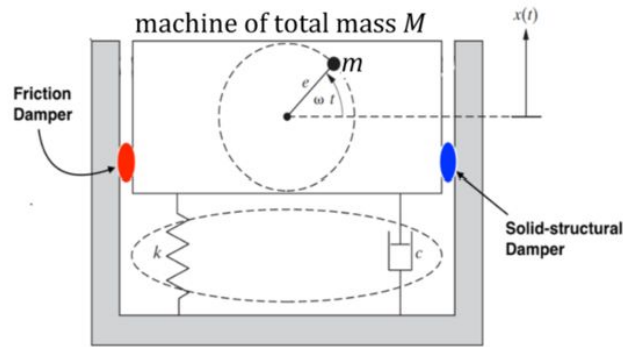
| Shaft Material→ | AISI 1018 | AISI 1030 | AISI 1040 |
|-----------------|-----------|-----------|-----------|
| Eccentricity↓ | | | |
| 0.5% | 25.46 | 24.06 | 23.68 |
| 1% | 27.74 | 26.59 | 26.30 |
| 1.5% | 29.89 | 28.46 | 28.30 |
| 2% | 32.31 | 30.92 | 30.04 |
| 2.5% | 34.21 | 32.91 | 31.44 |

As a result of the table above, eccentricity of 1% or more is dangerous for this design and can lead to fatigue failure. Also, it can be observed that the ultimate tensile strength of the material has a negligible impact on the diameter of the shaft.

Vibration Analysis of the system

In this study, we narrow our analysis to vibration induced by rotating parts on the device as a whole. The goal is to design a damper system to control the amplitude of vibration of the chamber when attached to the base. To simplify our analysis, the movement of the chamber is considered as a single degree of freedom in the plane that the components are rotating [rotation in z-axis, and movement of system in x-y plane]. The vibration's supporting pad can be modeled as a simple spring/damper system as shown in figure below:

Figure32: Schematic of the single degree of freedom system, vibration induced by rotational mass unbalance



The Vibration in the system has 2 parts. Vibration induced in the start-up period and while rotating in constant angular speed. From literature review, it is evident that the maximum amplitude of vibration happens at the moment that the start-up period finishes, or the torque drops to 0; and it is of significance to pay special attention to these instances. The general equation of motion during start up period can be presented as following:

$$M\ddot{x} + c\dot{x} + kx = me(\omega^2 \sin(\omega t) - \alpha \cos(\omega t)) . \quad (\text{Eq: 26})$$

Where M is the systems mass, c is damper coefficient, k is spring constant, me is unbalanced mass, ω is rotational speed, and α is angular acceleration.

However, as shown in above figure YY, in real life applications, other damper mechanism such as friction damper and solid-structural dampers will be used to reduce the vibration amplitude which changes the equation of motion to:

$$M\ddot{x} + c\dot{x} + kx + \beta . x . \dot{x} + \mu \dot{x} = me(\omega^2 \sin(\omega t) - \alpha \cos (\omega t)) \quad (\text{Eq: 27})$$

Where β is structural damping coefficient and μ is frictional damper coefficient.

To relate this study to our analysis, it is important to understand that it is near impossible to determine parameters such as spring and damper constant for the system unless the system is assembled and those values are measured. However, this analysis will determine that after those parameters are determined, what other dampers, with exact specifications can be purchased and added to the system to minimize the vibration amplitude. To do so, a Matlab code was developed that given values such as Systems Mass, Unbalanced mass, built in spring and damper coefficients, the code will return the acceptable value for frictional and structural dampers to keep the vibration amplitude below desired value.

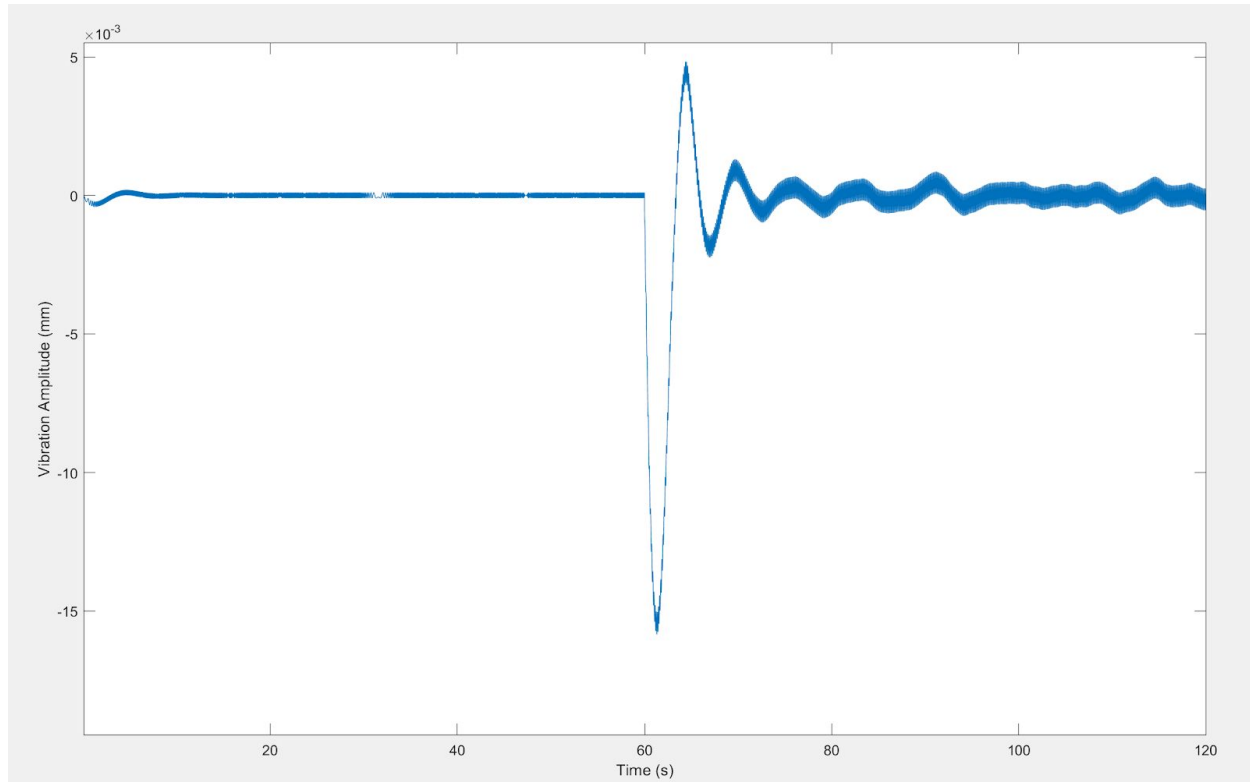
To illustrate how the Code functions, certain systems' parameters are assumed and their values are tabulated in the table below.

Table 17: Assumed values for Systems Vibration analysis

| Parameter | Value |
|--|-------------------------|
| Mass of system [M] | 50 Kg |
| Mass unbalance [me] | 0.05 Kg.m |
| Built in Spring [k] | 50 N/m |
| Built in damper [c] | 35 N.s/m |
| Targeted rotational speed [ω] | 995 $\frac{rad}{s}$ |
| Angular acceleration [α] | 16.59 $\frac{rad}{s^2}$ |
| Maximum desired vibration amplitude [Xmax] | 2 mm |

Given these values, the Code will simulate Vibration of the system for different Coefficient values for structural and frictional damper and return the combinations that pass the criteria of maximum vibration amplitude being less than 2mm. The simulation was run without any external dampers and the simulation's graph is shown in figure 33. Based on the results, it is shown that since the angular acceleration is fairly low, the vibration induced in the start-up period is minimal. It is also shown that the maximum vibration is induced when the start-up torque drops to 0, happening at $t=60$ sec and having vibration amplitude of 15mm. After that, the maximum vibration evident is approximately 3mm. The goal is to find some combinations of β and μ [coefficient of frictional and structural dampers] that reduces the maximum vibration amplitude of the system to below 2mm.

Figure 33: simulation of the systems' vibration without any external dampers



The simulations are run for combinations of $\mu=20:50$ and $\beta=20:50$, being frictional and structural dampers' coefficients respectively. Figure 34 shows the 3D plot of maximum vibration amplitude based on the values assumed for frictional[μ] and structural[β] dampers. The spikes in the figure essentially shows the combinations that do not pass the criteria. The reason for this phenomenon is that despite the general use of dampers for reducing vibration amplitude, combining them might constructively increase the effect of them on each other. Figure 36 shows that although the combination $\mu=45$, $\beta=23$ reduced vibration at the end of start-up period, it failed to reduce vibration amplitude when the device runs at constant speed. However, it reduced the vibration frequency by the order of 10^3 . In this analysis, the vibration frequency is not of significant importance; however, the simulation can also track this parameter in case it deems important. Figure 36 simply shows the combinations of μ and β that fail to pass the criteria for minimum vibration amplitude

Figure 34: z-axis is the vibration amplitude for different values of $[\mu$ and β].

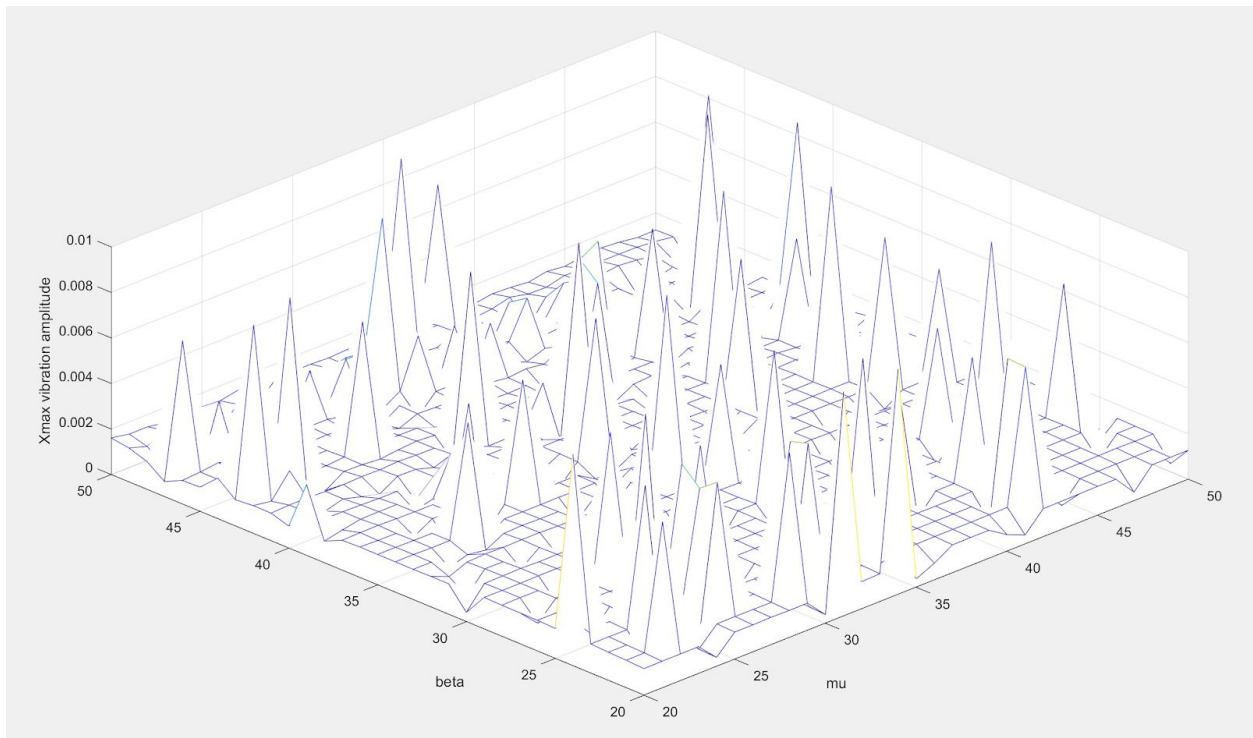


Figure 35: this figure shows the vibration of the system for $\mu=45$, $\beta=23$.

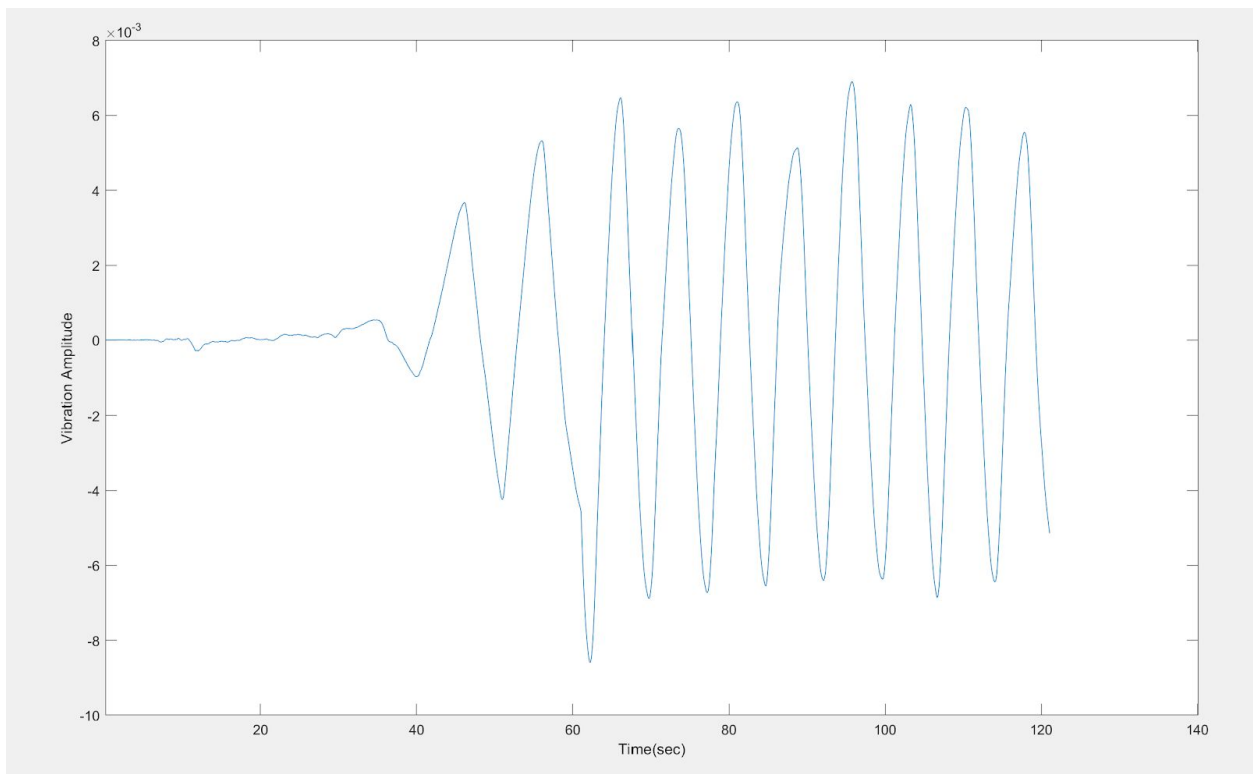
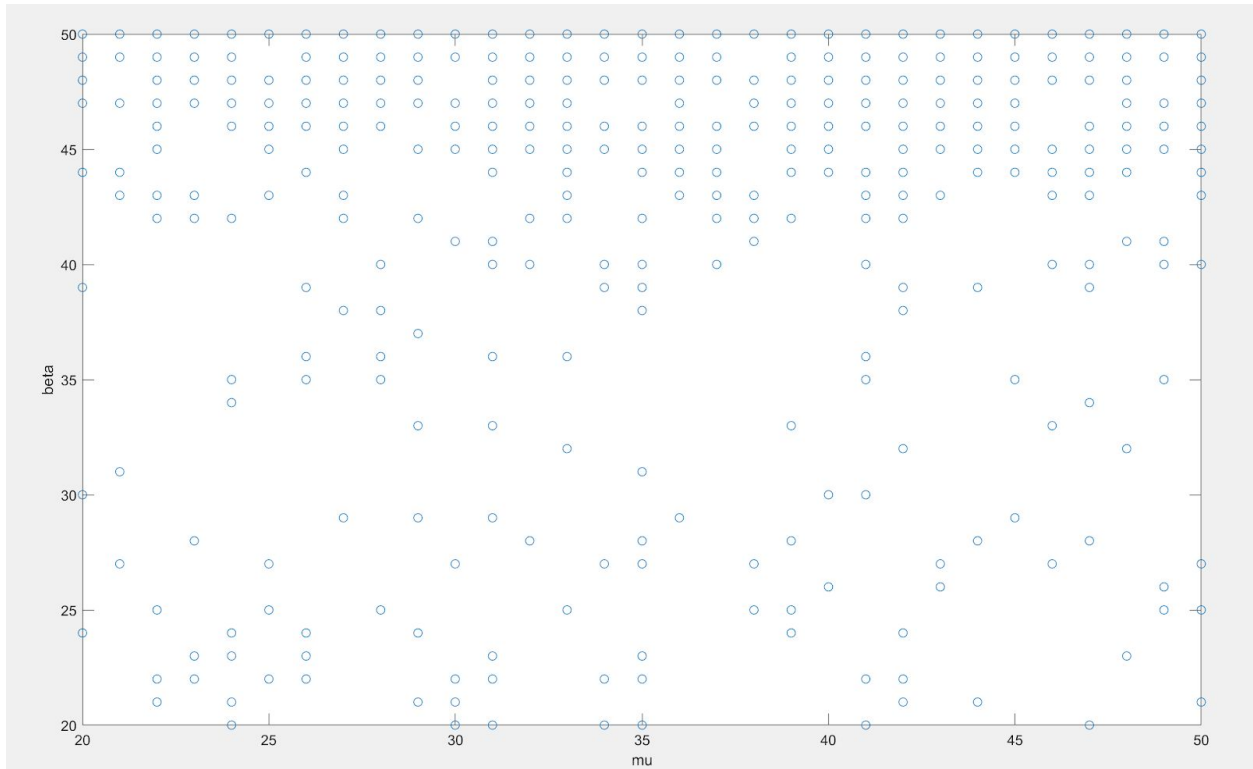


Figure 36: combinations of μ and β that do not pass the criteria



Based on the sample analysis done, it can be shown that after the design is manufactured and assembled, system's parameters such as frequency, spring and damper coefficients can be measured with instruments and the external damper system can be further designed to reduce the vibration of the device.

Below is the Code used to run the simulations and find the desired damper's coefficients:

```
function [t,tmax,x,Xmax,pass] = lab2(alpha,mu0,beta0)

% alpha: angular acceleration
% mu0: mu-array contains all mu values
% beta0: beta-array contains all beta values
% pass: array contains all (mu,beta) that meet the criteria
% Example:
% for (a), (b), [t,tmax,x,Xmax,pass] = lab2(alpha);
% for (d), [t,tmax,x,Xmax,pass] = lab2(alpha,mu0,beta0);
% where mu0, beta0 should be defined first.

if nargin==1
    mu0=0;
    beta0=0;
end
c=35;
k=50;
m=50;
me=0.02; % unbalance
om=995; % targeted rotating speed
tacc=om/alpha; % startup period

tspan=linspace(0,tacc+60,10000);
x0=[0;0];
opt=[];
idx=0;
pass=[];

for i=1:length(mu0)
    mu=mu0(i);
    for j=1:length(beta0)
        beta=beta0(j);
        [t,x]=ode45(@sdof,tspan,x0,opt,m,c,k,alpha,me,tacc,om,mu,beta);
        Xmax(i,j)=max(abs(x(:,1)));
        tmax(i,j)=t(abs(x(:,1))==Xmax(i,j));
        % check criteria (d1) max|x|?0.001 and (d2) 0.9*tacc ? tmax ? 1.1*tacc
        if Xmax(i,j) <= 0.005 && tmax(i,j)<=1.1*tacc && 0.9*tacc<=tmax(i,j)
            idx=idx+1;
            pass(idx,:)= [mu beta Xmax(i,j) tmax(i,j)];
            disp([mu beta]);
        end
    end
end
end
```

```

function G = sdof(t,x,m,c,k,alpha,me,tacc,om,mu,beta)

% students are to enter dxdt2 below. Note, for (a)~(c), the damping force
% in dxdt2 is -c*x(2), for (d), the coulumb and structural damping terms
% should be added; see explanations in lab sheet.

if t<tacc % startup period
    dxdt1=x(2);
    dxdt2=(-c*x(2)-mu*sign(x(2))-beta*sign(x(2))*abs(x(1))-k*x(1)+me*((alpha*t)^2*sin(alpha*t^2)-alpha*cos(alpha*t^2)))/m;
else
    dxdt1=x(2);
    dxdt2=(-c*x(2)-mu*sign(x(2))-beta*sign(x(2))*abs(x(1))-k*x(1)+me*om^2*sin(om*t))/m;
end
G=[dxdt1;dxdt2];

```

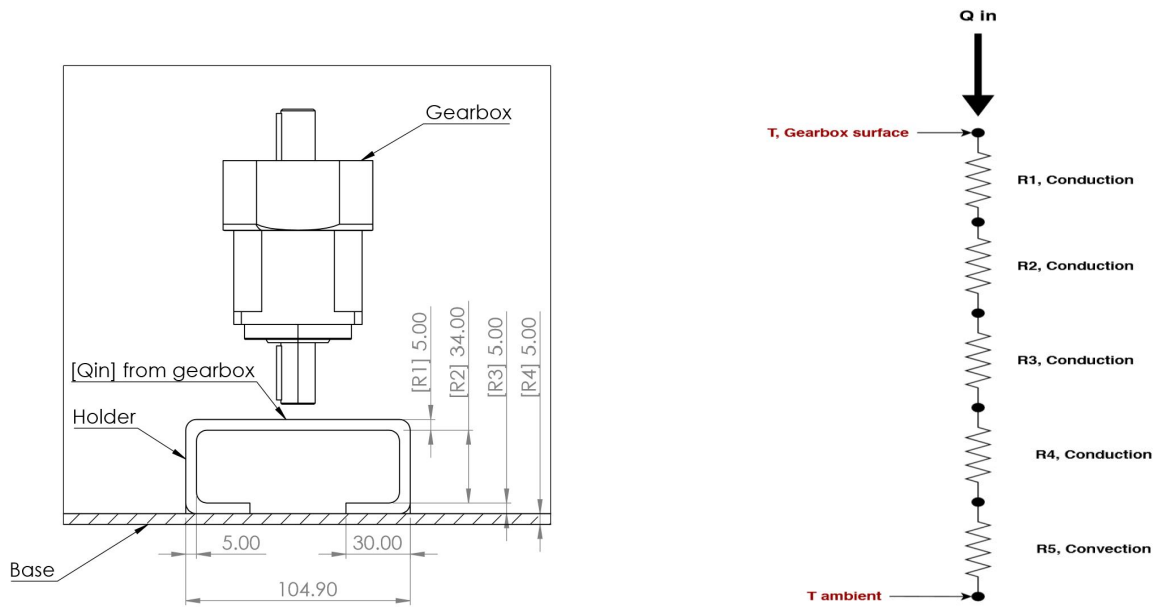
Heat transfer analysis on Gearbox

The heat transfer of the gearbox is particularly important since it is placed in a vacuum environment and the only method of heat transfer to ambient air is through conduction and radiation. To start our analysis, heat dissipation through radiation is neglected and will be analyzed if deemed important.

For this analysis, the ‘Thermal resistance method’ is utilized. Based on this concept, the ability of each component to transfer heat is considered resistance of the given component [R]. Given the rate of heat transfer through the system [Q_{in}] and ambient temperature [T_{ambient}], this concept can be used to obtain surface temperature of each component. Its equation is given below:

$$Q_{in} = \frac{T_H - T_{ambient}}{R_{network}} \quad (\text{Eq: 28})$$

Figure 37: The schematic of gearbox assembly and its corresponding conduction resistance network



Conduction and convection resistance can be calculated as following:

$$R_{conduction} = \frac{L}{k A} \quad (\text{Eq: 29})$$

$$R_{convection} = \frac{1}{h A_s} \quad (\text{Eq: 30})$$

Where L is the length of component, [A] is surface area of component, [k] thermal conduction coefficient, and [h] is thermal convection coefficient. As shown in figure 37, the gearbox is connected on a mount and the mount is further connected to the base which is exposed to ambient air. However, since the mount cross section changes, it is divided to 3 sections [R1, R2, R3] for this analysis. From equations above, the resistance of each component is calculated and tabulated in table below:

Table 18: Thermal resistance of components

| | R1 | R2 | R3 | R4 | R5 |
|--|--------------|------------|-------------|-------------|------------|
| Method of transfer | Conduction | Conduction | Conduction | Conduction | Convection |
| Area [A, m²] | 0.00789648 | 0.004049 | 0.00306192 | 0.00306192 | 0.00995501 |
| Length [L, m] | 0.005 | 0.034 | 0.005 | 0.005 | - |
| conduction coef [k, $\frac{W}{m.K}$] | 0.9 | 0.9 | 0.9 | 0.9 | - |
| convection coef [h, $\frac{W}{m^2.K}$] | - | - | - | - | 25 |
| Resistance [R, $\frac{C}{W}$] | 0.7035483602 | 36.0131342 | 1.814402583 | 1.814402583 | 4.01807733 |
| Total resistance [$\frac{C}{W}$] | 17.68058096 | | | | |

The amount of heat generated in the gearbox can be calculated as a percentage of total power transferred through the gearbox. The efficiency of the gearbox is rated at 95% which means 5% of the power transmitted will be converted to heat. Based on previous sections, the power transmitted through the gearbox can be calculated as :

$$P_{Total} = Torque \times Angular\ velocity = (0.026\ N.m) \times (950\ \frac{rad}{s}) = 24.7\ watt$$

$$\Rightarrow Q_{in} = 5\% \times P_{Total} = 1.235\ watt$$

Assuming ambient air at 25° , the surface temperature of the gearbox can be calculated as:

$$T_{gearbox} = T_{ambient} + Q_{in} \times R_{Total} = 46.834^{\circ}$$

This analysis shows that as the device runs, the heat generated in the gearbox causes the gearbox to warm up. However, the surface temperature does not exceed 50° which is a reasonable temperature for the gearbox to function at. It is also worthy to note that the radiation heat transfer was not considered in this analysis which further means that in reality a portion of the heat generated will be dissipated through radiation and the surface temperature will be held even lower than the value found.

9. Conclusion and Recommendation

The final design succeeded in meeting the major requirements of the project, such as particle speed, vacuum capability of appropriate value and durability of materials. The project also saw its optional requirement met. Naimly the acrylic viewing glass on top of the unit and the system's portability. Every component is mounted onto the unit itself and can be easily moved around a shop as needed. The weight however does limit its portability anywhere that height changes are required.

One of the main changes to the requirements was the use of a user interface. Since the motor comes with its own control system and driver, adding a custom user interface becomes prohibitive. Mainly the issue is that without having the driver in hand, designing a UI becomes a guessing game at best as we cannot test any of the designs on communicating with the motor driver.

The issue of fitting the correct sample size was tackled by allowing for adjustments on the fixtures holding the samples. Placing an object, as long as it was of size to fit into the chamber was not really an issue; it was aiming the unit correctly that was the problem. The added fixtures now allow samples to be fine tuned to be cut the fastest and most efficient in the unit.

An optional requirement was to limit the waste of abrasive. Considering that the abrasive trajectory is all around the chamber, we placed 4 sample holding fixtures to limit the waste. Also the blasters abrasive delivery system includes an auger that will stop the flow of abrasive when the device is off.

Finally there were no exact budgets set for the project but we strived to limit cost as much as possible. Any complex parts were taken from vendors, leaving the users' hands open to shop around if they need to and find cheaper parts, if possible. Other custom made parts were designed with simple geometry allowing any simple shop with a lathe or CNC to easily cut the needed parts.

As recommendations, the user must remember the unit is being operated under harsh conditions and as long as they keep within the materials used in the design no issues should come about. Also if the user does obtain the actual motor and driver they will be able to design a user interface for the unit. That being said the only control portion for the design in the motor itself and everything else works in tandem to the motors speed.

10. References

- [1] A. Ghobeity et al, "Process repeatability in abrasive jet micro-machining," *Journal of Materials Processing Tech*, vol. 190, (1), pp. 51-60, 2007.
- [2] P. J. Slikkerveer, P. C. P. Bouten and F. C. M. de Haas, "High quality mechanical etching of brittle materials by powder blasting," *Sensors & Actuators: A. Physical*, vol. 85, (1), pp. 296-303, 2000.
- [3] D. Aquaro, E. Fontani, Erosion of ductile and brittle materials, *Meccanica* 36 (2002) 651–661.
- [4] I.M. Hutchings, Ductile–brittle transitions and wear maps for the erosion and abrasion of brittle materials. *J. Phys. D* 25 (1992) A212–A221.
- [5] H. Wensink, M.C. Elwenspoek, Reduction of sidewall inclination and blast lag of powder blasted channels, *Sensors Actuators A Phys.*, 102 (1–2) (2002), pp. 157-164
- [6] A. Ghobeity, H. Getu, M. Papini, J.K. Spelt, Surface evolution models for abrasive jet micromachining of holes in glass and polymethylmethacrylate (PMMA), *J Micromech Microeng*, 17 (11) (2007), p. 2175
- [7] S. Shafagh and M. Papini, "The effects of blast lag in abrasive jet machined micro-channel intersections," *Precision Engineering*, vol. 62, pp. 162-169, 2020.
- [8] I. M. Hutchings, "Ductile-brittle transitions and wear maps for the erosion and abrasion of brittle materials," *Journal of Physics D: Applied Physics*, vol. 25, (1A), pp. A212-A221, 1992.
- [9] G. L. Sheldon and I. Finnie, "On the Ductile Behavior of Nominally Brittle Materials During Erosive Cutting," *Journal of Engineering for Industry*, vol. 88, (4), pp. 387, 1966.
- [10] J. A. C. Humphrey, "Fundamentals of fluid motion in erosion by solid particle impact," *International Journal of Heat and Fluid Flow*, vol. 11, (3), pp. 170-195, 1990
- [11] F. A. Salustri and W. P. Neumann. Creating a human-centric engineering design course. 2017.

[12]

https://deseng.ryerson.ca/dokuwiki/_detail/design:designspiralv1.png?id=design%3Adesign_process_overview

[13] Kohli, Rajiv Mittal, K.L.. (2016). *Developments in Surface Contamination and Cleaning, Volume 1 - Fundamentals and Applied Aspects (2nd Edition) - 14.4.4.1 Selection of the Abrasive*. Elsevier. Retrieved from

<https://app.knovel.com/hotlink/pdf/id:kt010SHNR1/developments-in-surface/selection-abrasive>

[14] “UAMA,” Unified Abrasives Manufacturers Association. [Online]. Available: <https://uama.org/abrasives-101/>. [Accessed: 12-Feb-2020].

[15] <https://www.comcoinc.com/wp-content/uploads/2016/07/NozzlePowder.pdf>

[16] Munkebo Clemco A/S, Munkebo, Denmark, www.munkebo.com.

[17] Marinescu, Joan D. Rowe, W. Brian Dimitrov, Boris Inasaki, Ichiro. (2004). *Tribology of Abrasive Machining Processes - 11.3.2 Synthetic Diamond*. William Andrew Publishing. Retrieved from

<https://app.knovel.com/hotlink/pdf/id:kt003I5FD5/tribology-abrasive-machining/synthetic-diamond>

[18] Gilbert, Jeremy. (2008). *Medical Device Materials IV - Proceedings from the 2007 Materials & Processes for Medical Devices Conference - 32.4 SEM & EDX Analysis*. ASM International. Retrieved from

<https://app.knovel.com/hotlink/pdf/id:kt00C21XA4/medical-device-materials/sem-edx-analysis>

[19] International Surface Preparation Canada. [Online]. Available: <http://www.surfaceprepcanada.ca/>. [Accessed: 13-Feb-2020].

[20] “Indian Institute of Technology Kanpur,” IITK. [Online]. Available: <http://home.iitk.ac.in/>. [Accessed: 13-Feb-2020].

[21] “Erosion Resistant coatings from Hardide Coatings,” Hardide Coatings. [Online]. Available: <https://hardide.com/properties/erosion-resistant-coating/>. [Accessed: 13-Feb-2020].

- [22] Upadhyaya, Gopal S.. (1998). Cemented Tungsten Carbides - Production, Properties, and Testing - 1.0 Corrosion. William Andrew Publishing/Noyes. Retrieved from <https://app.knovel.com/hotlink/pdf/id:kt00385R2A/cemented-tungsten-carbides/corrosion>
- [23] Lyons, William C. Plisga, Gary J. Lorenz, Michael D.. (2016). Standard Handbook of Petroleum and Natural Gas Engineering (3rd Edition) - 4.7.1.2 Roller Cone Bit Components. Elsevier. Retrieved from
- [24] L. Hofmann, "What is Durometer and Why is It Important?," Urethane Innovators, 29-Oct-2019. [Online]. Available: <https://urethaneusa.com/resources/what-is-durometer/>. [Accessed: 09-Apr-2020].
- [25] Manufacturing Guide Sweden AB. *Wheel blasting*. Retrieved from <https://www.manufacturingguide.com/en/wheel-blasting>
- [26] Essential Principles of Physics, P.M. Whelan, M.J. Hodgeson, second Edition, 1978, John Murray,
- [27] Pump World. *Lobe Positive Pump Type*. Retrieved from: <https://www.pumpworld.com/positive-displacement-pump-lobe-types.htm>
- [28] Zeluff, Mike. (2013). *Get the Most from Your Flexible Screw Conveyor - Tips for Successful Powder Processing*. Putnam Media. Retrieved from: https://www.chemicalprocessing.com/assets/wp_downloads/pdf/tips-for-successful-powder-processing.pdf
- [29] Boger, D. (2008). Move difficult-to-handle bulk materials with flexible screw conveyors. Chemical Engineering, 115(4), 36-39. Retrieved from <http://ezproxy.lib.ryerson.ca/login?url=https://search-proquest-com.ezproxy.lib.ryerson.ca/docview/194456734?accountid=13631>
- [30] Licari, J.J. Hughes, L.A.. (1990). *Handbook of Polymer Coatings for Electronics - Chemistry, Technology and Applications (2nd Edition) - Outgassing*. William Andrew Publishing/Noyes. Retrieved from <https://app.knovel.com/hotlink/pdf/id:kt001DHXD2/handbook-polymer-coatings/outgassing>
- [31] F. White, "Fluid Mechanics I," *Fluid Mechanics*, pp. 483–485.

- [32] T. Nagata et al, "Direct numerical simulation of flow around a heated/cooled isolated sphere up to a Reynolds number of 300 under subsonic to supersonic conditions," *International Journal of Heat and Mass Transfer*, vol. 120, pp. 284-299, 2018.
- [33] LACOTECH, "Vacuum Technology Solutions," *LACO Technologies*. [Online]. Available: <https://www.lacotech.com/>. [Accessed: 14-Feb-2020].
- [34] Panasonic Industrial Automation Sales, "MSMD082S1U," *DigiKey*. [Online]. Available: <https://www.digikey.ca/product-detail/en/panasonic-industrial-automation-sales/MSMD082S1U/1110-3723-ND/4302827>. [Accessed: 09-Apr-2020].
- [35] Parker, "ATEXGXAseries" *Parker*. [Online]. Available: <https://ph.parker.com/us/en/high-precision-inline-planetary-gearboxes-for-atex-applications-gxa-series/gxa3r005r0201>. [Accessed: 09-Apr-2020].
- [36] new air bearings , "NS - DF - 2 two face bearing " *New Seal*. [Online]. Available: https://www.newwayairbearings.com/wp-content/uploads/2019/07/NWAB_NEWSEAL_RACK_CARD_FINAL2020_WEB.pdf. [Accessed: 09-Apr-2020].
- [37] P. J. Slikkerveer, P. C. P. Bouten and F. C. M. de Haas, "High quality mechanical etching of brittle materials by powder blasting," *Sensors & Actuators: A. Physical*, vol. 85, (1), pp. 296-303, 2000.
- [38] R. G. Budynas, J. K. Nisbett, and J. E. Shigley, *Shigleys mechanical engineering design*. New York, NY: McGraw-Hill Education, 2020.

- Appendix A

-A1: code for calculating the drag experienced by the particles (MATLAB)

```
function [velocity] = particlespeed(Data,int_velocity,part_density)

for i=1:length(Data(:,1))
    density_flu=Data(i,1);
    diam=Data(i,2);
    coef=Data(i,3);
    area=((diam/2)^2)*pi();
    dist=0.01:0.01:7;
    F=coef*density_flu*(int_velocity^2)*area/2;
    mass=part_density*(pi()*(4/3)*(diam/2)^3);
    v_update=int_velocity;
    for j=1:length(dist)
        F=coef*density_flu*(v_update^2)*area/2;
        acc=F/mass;
        v_update=sqrt((v_update^2)-2*acc*0.0001);
        velocity(j,i)=v_update;
    end
end

end
```

The function above can be used as follows:

```
Data = load('Data.mat')
particlespeed(Data.Data,255,3290)
```

The Data mat file contains the following information:

Table 8: Illustrating the data mat file.

| Pressure [bar] | Particle diameter [m] | Coefficient of Drag |
|----------------|-----------------------|---------------------|
| 1.12 | 1E-5 | 0.86 |
| 0.02 | 1E-5 | 0.86 |
| 0.01 | 1E-5 | 0.86 |

-A2: code to calculate speed of impact of particles (Python)

The following code is the main.py file that is to be run.

```
# -*- coding: utf-8 -*-
"""
Created on Thu Jan 30 15:25:28 2020
This program is to test out the speed needed to cut.
The user can give different values for material properties
and abrasive mass.
@author: ssartipz
"""

import math
from reader import readCSV
import pandas as pd

class Mater:
    def __init__(self, C,K,E,H):
        self.C = C
        self.K = K
        self.E = E
        self.H = H
        self.Umin = self.energymin()

    def energymin(self):
        return ((self.C * (self.E**1.5) * (self.K**6)) / self.H**6.5)

class abras:
    def __init__(self, density, diam):
        self.dens = density
        self.diam = diam
        self.V = self.volume()
        self.m = self.mass()

    def volume(self):
        return (4/3) * math.pi * (self.diam/2)**3
```

```

def mass(self):
    return self.V * self.dens

def velocity(mass, energy):
    return math.sqrt(2*energy / mass)

#C          K          E          H
#material = Mater(2.4*10**5, 0.5*10**6, 52*10**9, 6*10**9)
#Fused Silica
if __name__ == "__main__":
    data = readCSV(plot = False)
    speedData = []
    for index, row in data.iterrows():
        material = Mater(2.3*10**4, row['fracture toughness (MPa)']*10**6,
                        row['elastic modulus (GPa)']*10**9,
                        row['Knoop hardness (GPa)']*10**9)
        abrasive = abras(3950, 10*10**-6)
        speed = velocity(abrasive.m, material.Umin)
        speedData.append({'Material' : row['ceramics'], 'speed' :
f"{speed:.3E} m/s"})
    df = pd.DataFrame(speedData)
    print(df)

```

The data functions that read in the csv data are given below and should be placed in the same directory as main.py and the csv file.

```

import pandas as pd
import numpy as np
import os
from pandas.plotting import table
import matplotlib.pyplot as plt

def readCSV(path = os.getcwd()+"\\GlassData.csv", plot = True):
    df = pd.read_csv(path, header = 0)
    if plot == True:

```

```

ax = plt.subplot(111, frame_on=False)
ax.xaxis.set_visible(False)
ax.yaxis.set_visible(False)

the_table = plt.table(cellText = np.array(df.iloc[0:,1:]),cellLoc
= 'center',
                      colWidths = [0.2]*np.shape(df.iloc[0,:])[0],
                      rowLabels = np.array(df.iloc[:,0]), colLabels =
np.array(df.columns[1:]),
                      loc = 9)

the_table.auto_set_font_size(False)
the_table.set_fontsize(10)

plt.show()

return df

```

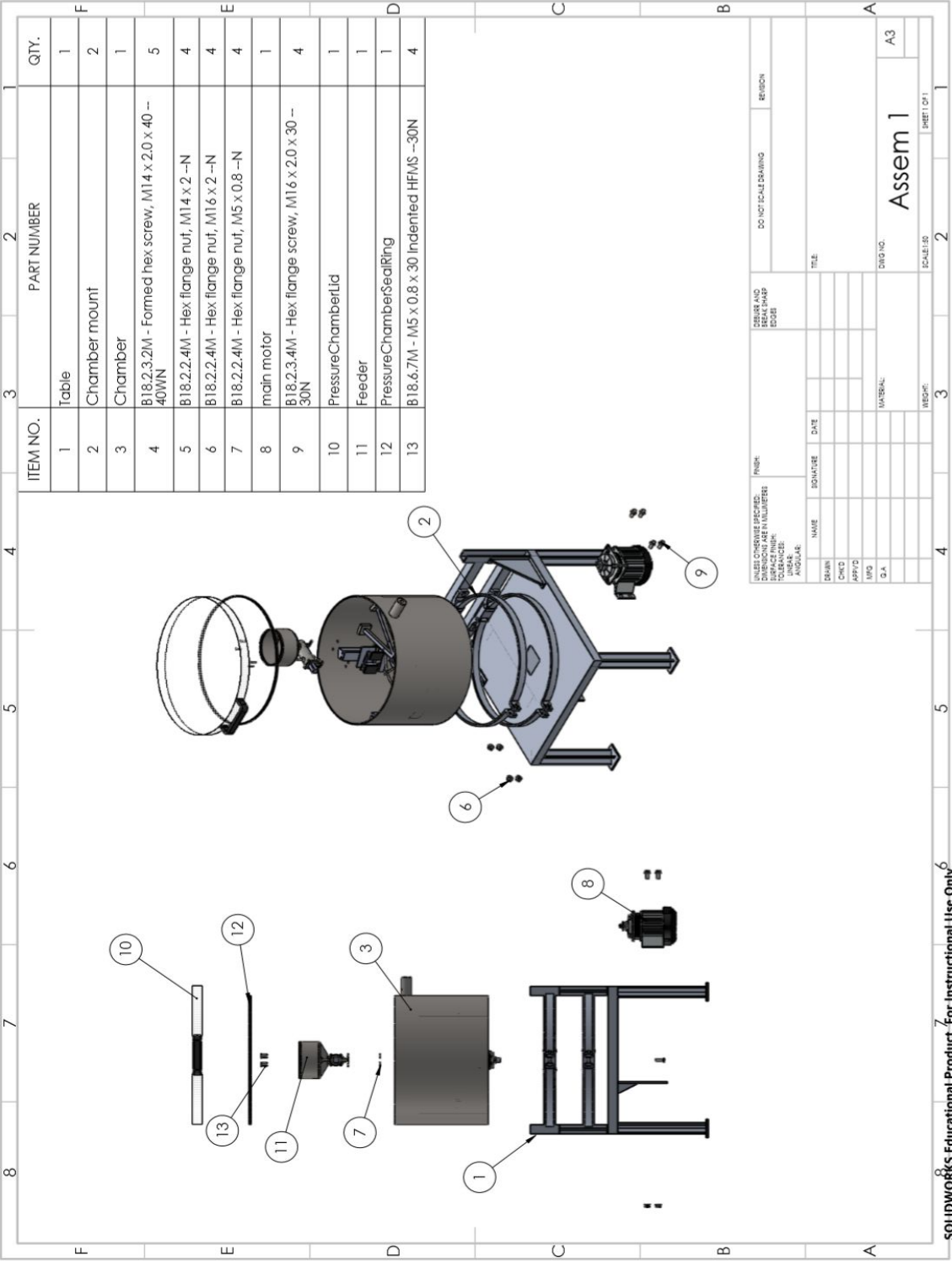
The Actual CSV file is listed below, and can be edited to the users liking.

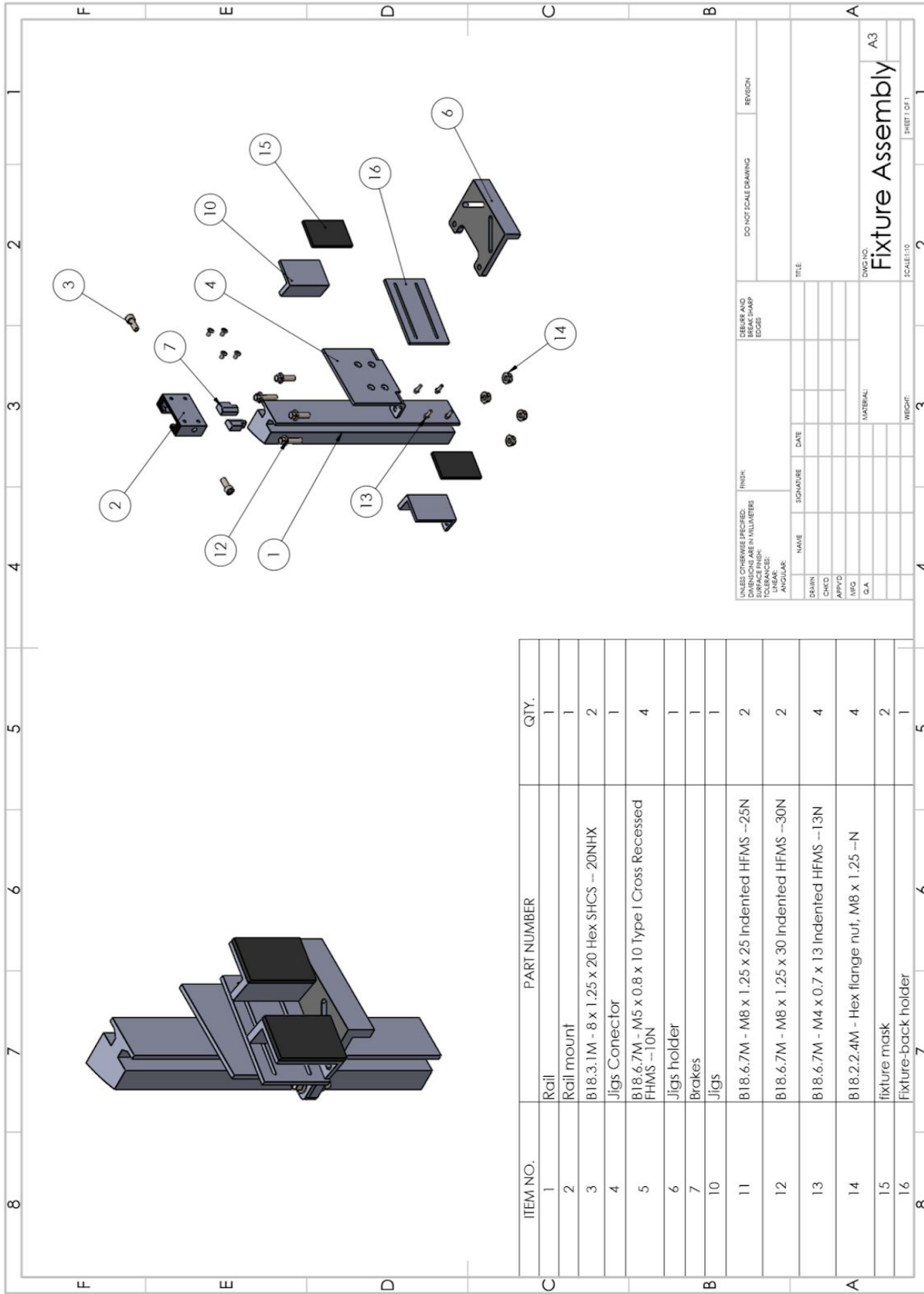
```

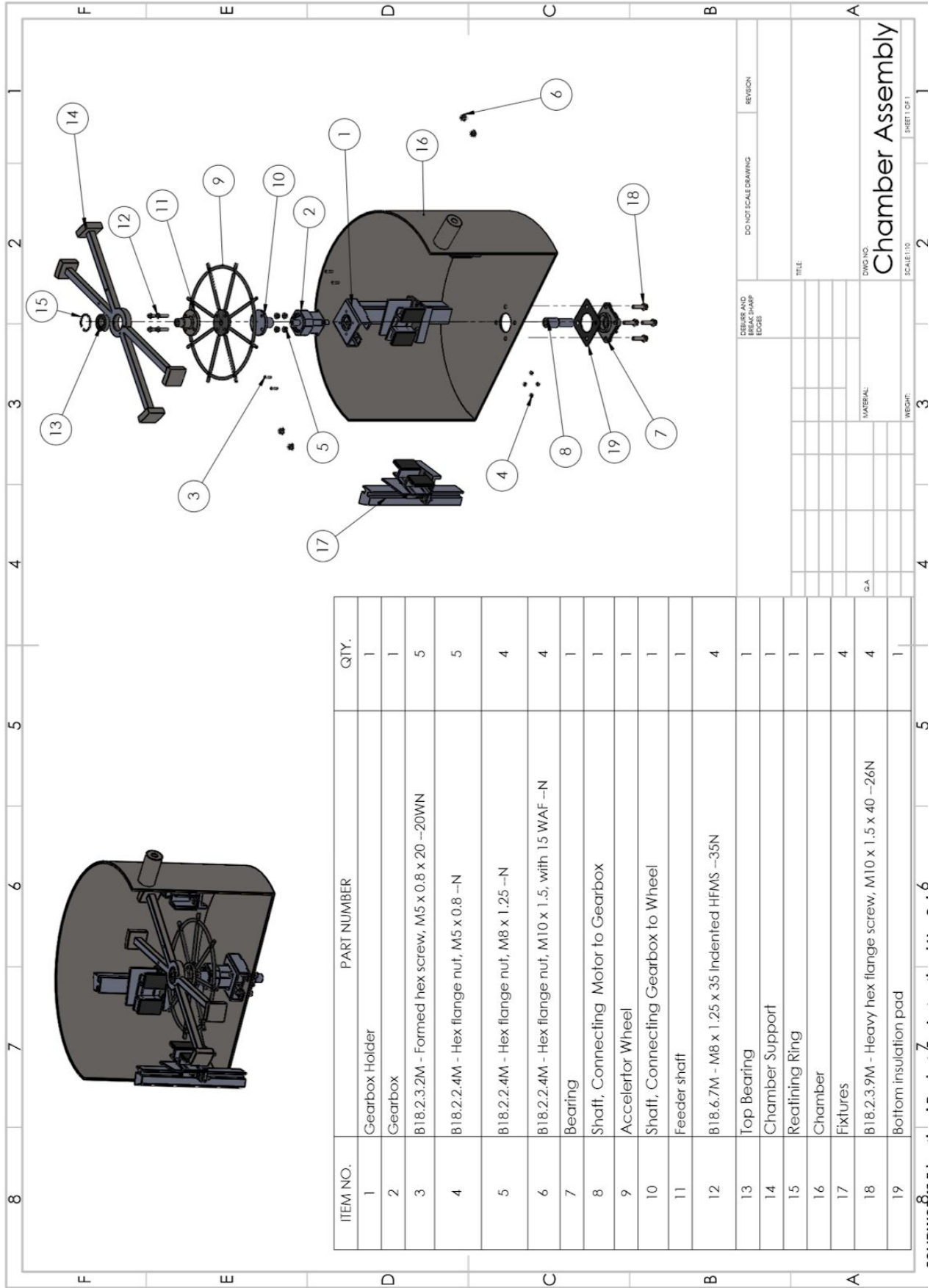
ceramics,density (kg/m3),elastic modulus (GPa),fracture toughness (MPa),Knoop hardness
(GPa),refractive index
Fused silica,2210,70,0.78,4.5,1.4585
Spinel,3590,268.5,1.7,13.5,1.7162
Aluminium oxynitride,3690,324.5,2.4,16,1.7983
Sapphire,3970,365,3.25,17.5,1.7681
poly crystalline alumina,3986,390,3.5,21.5,1.7682
Float glass,2500,72,0.65,5.72,1.5204
Glass ceramic,2400,65,0.71,6.33,1.5263
Quartz,2650,76.5,0.7,7.57,1.4586
Pyrex,2520,460,0.75,5,0
soda lime,2440,73.3,0.7,5.733,0
silicone carbide,3200,130,5,23.5,0
Borosilicate,2720,66.1,0.84,5.55,0

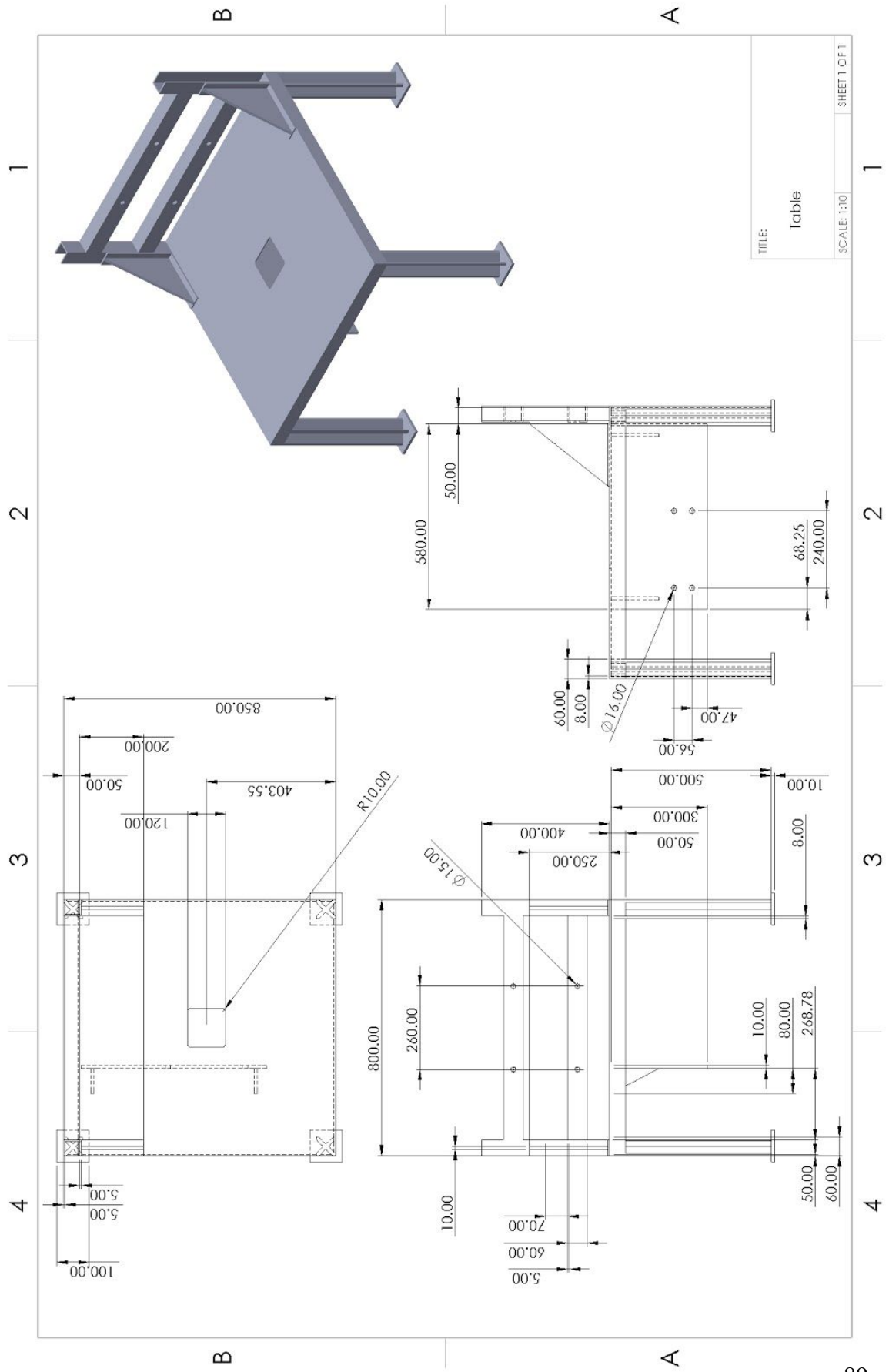
```

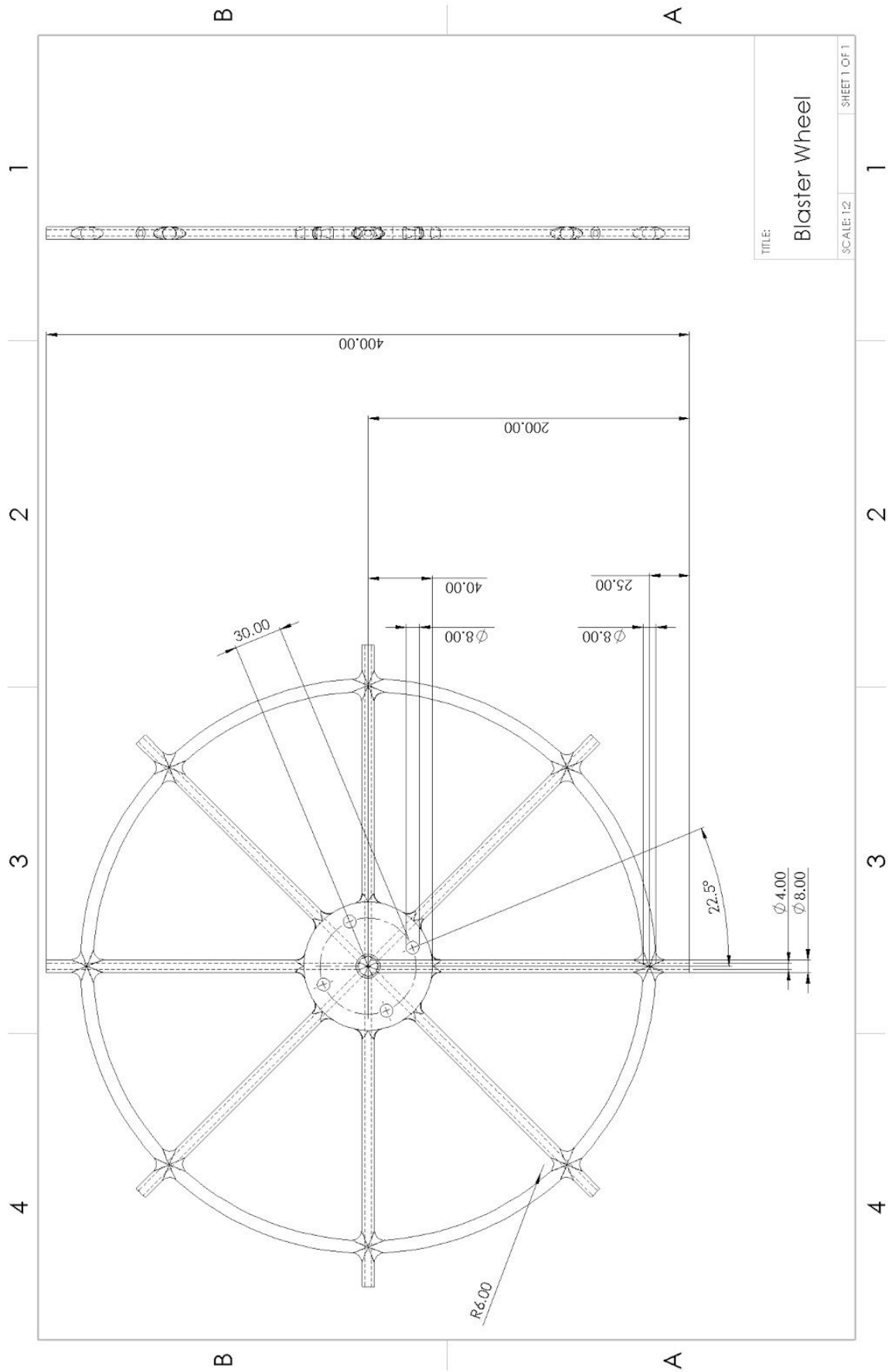
Appendix B: CAD Drawings











| | |
|--------------------------------|--------------|
| TITLE: Blaster Wheel | |
| SCALE: 1:2 | SHEET 1 OF 1 |

